M. Bartz, L.J. Arnold, M. Demuro, M. Duval, G.E. King, G. Rixhon, C. Álvarez Posada, J.M. Parés, H. Brückner

Single-grain TT-OSL dating results confirm an Early Pleistocene age for the lower Moulouya River deposits (NE Morocco)

Quaternary Geochronology, 2019; 49:138-145

Final publication at http://dx.doi.org/10.1016/j.quageo.2018.04.007

Single-grain TT-OSL dating results confirm an Early Pleistocene age for the lower Moulouya River deposits (NE Morocco)

M. Bartz[1*], L.J. Arnold[2], M. Demuro[2], M. Duval[3], G.E. King[4], G. Rixhon[5], C. Álvarez Posada[6], J.M. Parés[6] and H. Brückner[1]

[1] Institute of Geography, University of Cologne, Albertus-Magnus-Platz, 50923 Cologne/Germany

[2] School of Physical Sciences, Environment Institute, and Institute for Photonics and Advanced Sensing (IPAS), University of Adelaide, North Terrace Campus, Adelaide, SA, 5005/Australia

[3] Australian Research Centre for Human Evolution (ARCHE), Environmental Futures Research Institute (EFRI), Griffith University, 170 Kessels Road, Nathan, QLD 4111/Australia

[4] Institute of Geological Sciences, University of Bern, Baltzerstr. 1-3, 3012 Bern/Switzerland

[5] Laboratoire Image, Ville, Environnement (LIVE), UMR 7362 - CNRS, University of Strasbourg-ENGEES, 3 rue de l'Argonne, 67083 Strasbourg Cedex/France

[6] Centro Nacional de Investigación sobre la Evolución Humana (CENIEH), Paseo de Atapuerca, s/n, 09002 Burgos/Spain

*corresponding author: m.bartz@uni-koeln.de; +492214707719

Abstract

The lower Moulouya River (NE Morocco) drains a tectonically active area related to the NW-SE convergence of the African and Eurasian plates. Fluvial deposits preserved in the lower Moulouya have been dated to ~1.5-1.1 Ma as part of a recent multi-technique geochronology study. The present work aims to verify and refine the existing Early Pleistocene (~1.8-0.8 Ma) ages for the Moulouya deposits using single-grain thermally transferred-OSL (TT-OSL) dating. The single-grain TT-OSL D_e distributions are characterised by high overdispersion (77-91 %), significant negative skewness, and several discrete populations can be identified when applying the finite mixture model (FMM). The lowest FMM dose components of the TT-OSL datasets comprise relatively dim grains that have very slow decays. The Fast Ratio (FR) was therefore used to explore whether the presence of slower-decaying TT-OSL components might have exerted a significant effect on our D_e values. Our samples show a 40-50 % increase in weighted mean D_e and a 50-100 % decrease in overdispersion when applying a FR acceptance threshold of 2, resulting in the elimination of the lowest FMM component. Application of a higher FR value does not result in any additional change in TT-OSL D_e value. Dose recovery tests confirm the suitability of the single-grain TT-OSL protocol and use of an additional FR acceptance threshold of ≥2 for final age determination. Previous geomorphic interpretations suggested a capture event occurred at the Beni Snassen gorge between 1.04 and 1.36 Ma at the latest. This interpretation is supported by the newly obtained TT-OSL ages, which reveal that fluvial deposition occurred between ~1.09 and ~1.15 Ma.

Keywords: Quartz, single-grain, TT-OSL, fluvial terraces, Morocco

1. Introduction

The Moulouya River (~74.000 km^2; Fig. 1a), drains an active tectonic setting resulting from the collision between the Eurasian and African plates, which leads to a complex geodynamic background in this convergence zone (Meghraoui et al., 1996; Barcos et al., 2014). Along the ~600 km-long Moulouya drainage, the sedimentary infill (including Quaternary fluvial deposits) of the lowermost Neogene basin (the so-called Triffa basin) is thus strongly deformed along a sub-continuous W-E striking thrust zone (Rixhon et al., 2017; Fig. 1b). As for the geochronology of the lower Moulouya, in addition to ^{14}C dating of the Holocene sedimentary record (e.g., Zielhofer et al., 2010), a recent study based on a combination of electron spin resonance (ESR) dating of quartz using the multiple centres (MC) approach, post-infrared infrared (pIRIR) stimulated luminescence dating of K-feldspar, and ~~palaeomagnetic analysis~~magnetostratigraphy has yielded a reliable framework for the Pleistocene terrace deposits (Bartz et al., 2018). ESR numerical ages, all clustering between ~1.1 and 1.5 Ma, are supported by a reversed polarity in almost all river profiles; the presumed absence of Middle Pleistocene river sediments in the Triffa basin seems to rule out climate as the main driver for fluvial deposition (Bartz et al., 2018).

Against this background, the present study aims to verify and refine the existing chronostratigraphy of the lower Moulouya using single-grain thermally transferred-OSL (TT-OSL) dating. TT-OSL dating (Wang et al., 2006) makes use of a quartz luminescence signal that saturates at much higher radiation doses than the conventional OSL signal. In sedimentary archives, the TT-OSL signal has mostly been applied to aeolian (e.g., Stevens et al., 2009; Yi et al., 2012), marine (e.g., Jacobs et al., 2011) and archaeological (e.g., Sun et al., 2013; Demuro et al., 2014; Arnold et al., 2015) deposits spanning Early and Middle Pleistocene timescales. Nevertheless, establishing reliable TT-OSL chronologies over such 'extended' age ranges has often proved challenging due to a number of complications with multi-grain TT-OSL signal characteristics (e.g., signal sensitivity, bleachability, thermal stability; Duller and Wintle, 2012).

Recently, single-grain TT-OSL dating has been reliably applied to several independently or semi-independently dated sedimentary archives (e.g., Arnold et al., 2014; Demuro et al., 2015). For samples with sufficiently bright signals, single-grain TT-OSL offers a number of potential advantages over multi-grain TT-OSL approaches; particularly the ability to isolate grains with favourable TT-OSL properties, the detection of inter-grain differences in problematic TT-OSL behaviours (including low thermal stabilities), and a means of circumventing averaging effects arising from simultaneously measuring grains with different bleaching histories, signal compositions or TT-OSL source trap properties (Arnold et al., 2014; Arnold and Demuro et al., 2015; Arnold et al., this volume). In the fluvial context, Arnold et al. (2013) compared the suitability of both single-grain and multi-grain TT-OSL dating on deposits from the Pico River in northern Spain, obtaining consistent ages of ~350 and ~330 ka, respectively. These TT-OSL ages were in agreement with ESR quartz ages, based on the aluminium centre, from adjacent river terraces (Moreno et al., 2012). Single-grain TT-OSL therefore offers a potentially viable means of dating the Moulouya quartz samples and may help further understand the Early Pleistocene depositional history.

2. Sampling and luminescence dating procedures

Four >20 m-thick fluvial sections were investigated by Bartz et al. (2018) in the Triffa basin, the so-called BOU, DOE, MRB and TOLL profiles (see Figs. 1b and 2). The initial geochronological framework was based on the MC approach in ESR dating, which involved measuring both the Al and Ti centres in each quartz sample (Fig. 2). The ages obtained using this approach were consistent with reversed magnetic polarities found in the fluvial deposits (Bartz et al., 2018), and revealed that fluvial aggradation took place between ~1.5 and ~1.1 Ma (Fig. 2). In addition, post-infrared infrared (pIRIR) stimulated luminescence measurements undertaken as part of the same study showed that both the $pIRIR_{225}$ and $pIRIR_{290}$ signals were saturated, yielding minimum ages between ~0.39 and ~0.80 Ma (Bartz et al., 2018).

In this study, two samples from the BOU section (C-L3824 and C-L3825) were investigated to test the applicability of single-grain TT-OSL (Fig. 2), which may yield non-saturated signals over these timescales and thus may provide further numerical age constraint on fluvial deposition in the Moulouya basin.

Sample preparation for luminescence dating was undertaken at the Cologne Luminescence Laboratory (CLL), University of Cologne. Single-grain TT-OSL measurements (Arnold et al., 2014) were made at the Prescott Environmental Luminescence Laboratory, University of Adelaide. Full details of the sample preparation, measurement equipment and protocol (Tab. S1), as well as the laboratory experiments employed in this study, are provided in the supplementary material. Radionuclide data and dose rates (Tab. S2) for all samples are presented in supplementary material.

The equivalent dose (D_e) quality assurance criteria used as part of the single-grain TT-OSL dating procedures followed Arnold et al. (2014). Grains were rejected from consideration if they displayed: (i) T_n <3σ background; (ii) Recycling ratio ≠ 1 at ±2σ; (iii) 0 Gy L_x/T_x >5% L_n/T_n ; (iv) OSL-IR depletion ratios <1 at ±2σ (Duller, 2003); (v) Non-intersecting grains (L_n/T_n > dose response curve saturation); (vi) Saturated grains ($L_n/T_n \geq$ dose response curve I_{max} at ±2σ); (vii) Extrapolated grains (L_n/T_n > highest L_x/T_x at ±2σ) and (viii) Anomalous dose response / unable to perform Monte Carlo fit.

~~The Fast Ratio (FR) (see also supplementary material)~~The Fast Ratio (FR) (Durcan and Duller, 2011; Duller, 2012) has been applied to the two BOU samples to provide a proxy for TT-OSL charge transfer into the fast OSL component trap relative to the medium and slow OSL component traps, as well as for identifying the dominance of potentially interfering (non-transferred) residual slow OSL components in the TT-OSL signals (see Supplementary material). The FR has been calculated by comparing the counts in the initial part of the TT-OSL decay curve (L_1) with those in the middle part of the decay (L_2) after subtracting a late light background count (L_3) according to the equation $(L_1\text{-}L_3)/(L_2\text{-}L_3)$. The FRs for our single-grain D_e datasets were calculated using the approach described in Duller (2012), but with the integration intervals specified by Jacobs et al. (2013) (i.e., the first 0.017 s for the L_1, 0.170-0.221 s for L_2 and the last 0.068 s for L_3), since these are based on the 90 % laser power used in the present study. Progressively higher FR thresholds have been applied to the single-grain TT-OSL D_e datasets, starting at a FR of 0 and increasing in FR increments of 0.5 until the culled dataset contained fewer than 10 individual D_e values (i.e., the sample size became too limited to ensure precise single-grain D_e determination). In each instance, grains were only accepted for further D_e analysis if their individual FR value equalled or exceeded the corresponding FR threshold.

A single-grain TT-OSL dose-recovery test was performed on a batch of 1000 unbleached grains of sample C-L3824 owing to the long durations of light exposure needed to bleach natural TT-OSL signals down to low residual levels (e.g., Demuro et al., 2015; Arnold et al., this volume). A known (941 Gy) laboratory dose of similar magnitude to the expected D_e was added on top of the natural signal for these grains. The expected D_e was initially determined by undertaking a sub-set of natural D_e measurements on 300 grains of sample C-L3824 prior to performing the dose-recovery test. The recovered dose was ~~then~~ calculated by subtracting the weighted mean natural D_e of sample C-L3824 (i.e., as shown in Table 1 determined from 1600 grains) from the weighted mean D_e of the unbleached and dosed grains.

3. Results and discussion

3.1 Single-grain TT-OSL properties and dose distributions

Between 1000 and 1600 single-grain TT-OSL D_e measurements were made on samples C-L3824 and C-L3825. Application of the SAR quality assurance criteria of Arnold et al. (2014) resulted in 2–4 % of measured D_e values being accepted for age calculation (Tab. S3). The vast majority of remaining D_e values (86-88 %) were eliminated for having very weak T_n signals (<3σ background), with smaller populations rejected for having poor recycling ratios that were not consistent with unity at 2σ (3 %) and anomalous/scattered dose-responses that could not be fitted with the Monte Carlo procedure (7 %). The TT-OSL decay curves of accepted grains have relatively low T_n intensities of 50–2000 cts/0.17 s, and the corresponding dose response curves are generally well represented by a single saturating exponential fitting function with ~~high~~ D_0 values of 10^2-10^3 Gy (Fig. 3).

The single-grain TT-OSL D_e distributions (Fig. 4) are characterised by high overdispersion values of 77-91 % (Tab. S4), which are well above the average reported value for 'ideal' single-grain TT-OSL samples (21±2 %; Arnold et al., this volume). Both D_e distributions are significantly negatively skewed according to the criteria outlined by Arnold and Roberts (2009) (Tab. S4), and both datasets contain several discrete dose populations when fitted with the finite mixture model (FMM; Galbraith and Green, 1990) (Fig. 4a, c). The dominant FMM components (i.e., those containing the highest proportion of individual D_e values; n = ~~27~~34 and ~~34~~27 grains for C-L3824 and C-~~L3824~~L3825, respectively) yield ages in agreement with the ESR dating estimates of ~1.1-1.3 Ma for BOU (Bartz et al., 2018) (Fig. 2). However, the lower dose FMM components underestimate the existing site chronology by 68-96 % (Tab. S4). Similar low dose components were observed in the Early Pleistocene single-grain TT-OSL study of Arnold and Demuro (2015), and were attributed to inter-grain variations in TT-OSL signal characteristics. Given the well-stratified nature of these fluvial deposits, it seems unlikely that post-depositional mixing could explain the multi-modal D_e distributions of samples C-L3824 and C-L3825. Similarly, beta dose heterogeneity is unlikely to give rise to such extreme and discrete low dose components in most typical sedimentary contexts (e.g., Nathan et al., 2003; Guérin et al., 2013). It seems possible therefore, that intrinsic sources of D_e scatter may partly or wholly explain these complex single-grain TT-OSL datasets.

Several of the accepted grains from samples C-L3824 and C-L3825 display very slowly decaying TT-OSL signals (i.e., T_x signals that did not reach background after 2 s of laser stimulation) (e.g., Fig. 3d). Such slow-decay dominated signals have been shown to be associated with potentially problematic TT-OSL behaviours (poor dose recovery test results, inferior thermal stabilities, experimentally sensitised components and unreliable TT-OSL D_e estimates) for some samples (e.g., Tsukamoto et al., 2008; Brown and Forman, 2012; Arnold and Demuro, 2015; Demuro et al., 2015). It may therefore be appropriate to introduce an additional signal quality assurance criterion to remove these slowly decaying signals, which we explore in the following sections.

3.2 Application of single-grain Fast Ratios (FR)

To examine whether TT-OSL charge transfer into slowly bleaching OSL traps or the presence of interfering (non-transferred) slow OSL signal components might have exerted a significant effect on our D_e datasets, we calculated single-grain Fast Ratios (FR) (Durcan and Duller, 2011; Duller, 2012) using the approach described in Demuro et al. (2013). Although TT-OSL signals are thermally transferred from a different source trap into the conventional OSL dating trap, any unfavourable behaviour associated with the latter (i.e., medium or slow component dominance, and hence low FR value) or interference from additional (non-conventional) OSL traps may be indicative of potentially unsuitable quartz behaviour.

The range of FRs obtained for our TT-OSL datasets (0.2–54) are lower than those reported for single-grain OSL datasets (e.g., 1.1–108 in Demuro et al., 2013). The lowest individual D_e values (<300 Gy) in both datasets yield correspondingly low FR values (Fig. 5a). In order to examine the potential of using the FR as an additional rejection criterion for single-grain data analysis, we applied increasingly stringent FR thresholds to the accepted D_e datasets, and examined the effects on weighted mean D_e and overdispersion (Fig. 5b-c). Both samples show a 40-50 % increase in weighted mean D_e and a 50-100 % decrease in overdispersion when applying incrementally higher FR acceptance thresholds between 0 and 2. Use of more stringent FR acceptance ratios >2 has no further discernible effect on D_e or overdispersion, other than causing a fourfold reduction in the number of accepted grains (Fig. 5b-c). These results suggest that slow decaying TT-OSL grains with FRs <2 exert an influence on the single-grain TT-OSL datasets. It may therefore be beneficial to employ an additional SAR quality assurance criterion based on a FR threshold of ≥2 for these samples. This is supported by the resultant D_e distribution characteristics and FMM fitting results shown in Fig. 4b, d. Application of a FR acceptance threshold of ≥2 results in the elimination of the lowest FMM component for both samples. The revised D_e distribution of C-L3824 is no longer considered to be significantly negatively skewed, has an overdispersion of 0 %, and is well represented by a single dose population centred on the central age model (CAM) D_e value (Galbraith et al., 1999; Tab. S4). The initially identified low dose FMM component for this sample therefore seemingly originated from grains with slowly decaying TT-OSL signals that are poorly suited to being measured with a SAR protocol. The revised D_e distribution of C-L3825 retains one of the two originally identified low dose FMM components and is still considered to be negatively skewed. However, its overdispersion is reduced by 50 % and the dominant FMM component now accounts for a significant proportion (~80 %) of measured grains (Tab. S4). The latter has therefore been used to derive the final age for this sample. ~~As with sample C-L3824, it seems that the initially identified FMM K_1 dose component originated from grains with slowly decaying TT-OSL signals.~~ The minor low dose FMM component remaining after applying the FR ≥2 acceptance threshold potentially originates from other sources of intrinsic D_e scatter (e.g., fast-dominated grains that do not respond well to the SAR conditions or grains with thermally unstable TT-OSL signals) or unidentified extrinsic D_e scatter. As with sample C-L3824, it seems that the initially identified FMM K_1 dose component originated from grains with slowly decaying TT-OSL signals.

3.3 Dose recovery results

A TT-OSL dose recovery test performed on C-L3824 (Fig. S1) attests to the general suitability of the single-grain TT-OSL protocol and use of an additional FR acceptance threshold of ≥2 for final age determination. The FR characteristics and D_e distribution of the unbleached and dosed grains mirror those obtained for the natural D_e dataset of C-L3824 (Fig. S1). The low dose FFM component observed for the unbleached and dosed dataset also lies significantly below the administered dose of 941 Gy, confirming an intrinsic rather than extrinsic origin for the D_e scatter. A net (i.e., natural-subtracted) recovered-to-given ratio of 1.04±0.07 and an overdispersion value of 0 % was obtained for the unbleached and dosed grains of this sample when applying a FR acceptance threshold of ≥2.

3.4 Consolidating the chronostratigraphy for the Lower Moulouya fluvial terraces

The single-grain TT-OSL ages obtained for the uppermost part of the BOU section are stratigraphically consistent: the lowermost sample (C-L3824) yielded an age of 1.09±0.10 Ma, while the upper sample (C-L3825) provided an age of 1.15±0.10 Ma (Fig. 2). The two new numerical ages are consistent at 1σ with the corresponding ESR ages of 1.26±0.10 and 1.10±0.11 Ma (Tab.1) derived from the same samples, and the reversed magnetic polarities identified at this section (Bartz et al., 2018). When combined with the existing ESR ages and ~~palaeomagnetic analyses~~magnetostratigraphy, the new TT-OSL data provide a refined chronological framework for the evolution of the Moulouya terraces during the Early Pleistocene. Collectively, the former and new numerical age estimates unequivocally point to the occurrence of a major depositional event in the lowermost sedimentary basin during the Matuyama chron (>0.77 Ma; Okoda et al., 2017). The chronologies developed in this study strongly supports many of the geomorphological interpretations previously reached by Bartz et al. (2018). In particular, they confirm the time span over which the assumed capture event took place through the uplifting Beni Snassen (i.e., linking the Guercif and Triffa basins via the Beni Snassen gorge; Bartz et al., 2018); that is between 1.05 and 1.25 Ma at the latest (according to the TT-OSL age provided by the upper sample C-L3825). They also demonstrate the usefulness of cross-checking ages obtained from independent dating methods to establish a particularly robust chronological framework for reconstructing long-term landscape evolution.

3.5 Reliability of the single-grain TT-OSL ages

In assessing the reliability of the final single-grain TT-OSL ages, it is worth briefly considering two issues: (i) the slow optical resetting rates of TT-OSL signals and the potential retention of unbleached residuals prior to deposition; (ii) the possible need for applying a thermal stability correction when applying TT-OSL signal over extended burial periods. The recent modern analogue study by Arnold et al. (this volume) revealed single-grain TT-OSL residual doses of 0-24 Gy for comparable dryland fluvial deposits from Spain and Australia. Such residual D_e values would be largely insignificant over the burial dose ranges considered here, and would be well within the existing 2σ TT-OSL D_e uncertainties for samples C-L3824 and C-L3825. Reported lifetime estimates for TT-OSL signals are highly variable (e.g., Adamiec et al., 2010; Brown and Forman, 2012) and have been exclusively derived using multi-grain TL loss and isothermal decay datasets. Arnold and Demuro (2015) have shown that multi-grain assessments of TL signal loss may provide limited insights into single-grain TT-OSL source trap lifetimes due to averaging effects, the dominance of grain populations that do not produce TT-OSL, and interference from slowly bleaching OSL components. As we cannot be confident that existing (multi-grain aliquot) laboratory lifetime predictions are of direct relevance to the specific grain populations isolated in our single-grain analysis, we have not applied an additional thermal stability correction to the final TT-OSL ages. This decision appears to be supported by the consistency of the single-grain TT-OSL and ESR ages at BOU (cf., Bartz et al., 2018), which suggests that any potential age underestimations related to thermal instability are not significant beyond the existing uncertainty ranges of our final chronologies.

4. Conclusion

The existing geochronological framework for the lower Moulouya terraces, which is based on a combination of ESR, pIRIR and palaeomagnetism (cf., Bartz et al., 2018), has been successfully verified by quartz single-grain TT-OSL dating in this study. The consistency between the newly obtained single-grain TT-OSL ages and the existing ESR and palaeomagnetism chronologies is particularly encouraging, and it indicates that massive fluvial deposition occurred in the lower Moulouya towards the end of the Early Pleistocene. Whilst application of conventional OSL and pIRIR dating remains unsuccessful over Early Pleistocene timescales due to signal saturation, our results show that single-grain TT-OSL can successfully be applied over extended age ranges in some settings. The TT-OSL ages presented in this study are the oldest published so far and their reliability is supported by independent dating evidence. Importantly, suitable D_e determination was only achievable for these samples after undertaking grain-specific assessments of TT-OSL signal variability, and applying an additional quality assurance criterion based on a FR acceptance threshold of ≥2. This may not have been possible, at least to the same extent, if we had employed conventional, multi-grain TT-OSL dating on these fluvial deposits.

Acknowledgements

This project is affiliated to the CRC 806 "Our Way to Europe", which is generously funded by the German Research Foundation [DFG; Grant-No.: SFB 806/2]. The support by the "Institut National des Sciences de l'Archéologie et du Patrimoine du Maroc" (INSAP) and by the "Commission for Archaeology of Non-European Cultures" (KAAK) of the German Archaeological Institute (DAI) is gratefully acknowledged, in particular of Abdeslam Mikdad and Josef Eiwanger, respectively. Aspects of the study have been funded by Australian Research Council Grant FT130100195 awarded to Lee J. Arnold, FT150100215 awarded to Mathieu Duval and DE160100743 awarded to Martina Demuro. Georgina E. King acknowledges support from Swiss National Science Foundation grant number PZ00P2-167960.

References

Adamiec, G., Duller, G.A.T., Roberts, H.M., Wintle, A.G., 2010. Improving the TT-OSL SAR protocol through source trap characterisation. Radiation Measurements 45, 768-777.

Arnold, L.J., Roberts, R.G., 2009. Stochastic modelling of multi-grain equivalent dose (D_e) distributions: Implications for OSL dating of sediment mixtures. Quaternary Geochronology 4, 204-230.

Arnold, L.J., Demuro, M., Navazo, M., Benito-Calvo, A., Pérez-González, A., 2013. OSL dating of the Middle Palaeolithic Hotel California site, Sierra de Atapuerca, north-central Spain. Boreas 42, 285-305.

Arnold, L.J., Demuro, M., Parés, J.M., Arsuaga, J.L., Aranburu, A., Bermudéz de Castro, J.M., Carbonell, E., 2014. Luminescence dating and palaeomagnetic age constraint on hominins from Sima de los Huesos, Atapuerca, Spain. Journal of Human Evolution 67, 85-107.

Arnold, L.J., Demuro, M., 2015. Insights into TT-OSL signal stability from single-grain analyses of known-age deposits at Atapuerca, Spain. Quaternary Geochronology 30, 472-478.

Arnold, L.J., Demuro, M., Parés, J.M., Pérez-González, A., Arsuaga, J.L., Bermúdez de Castro, J.M., Carbonell, E., 2015. Evaluating the suitability of extended-range luminescence dating techniques over early and Middle Pleistocene timescales: Published datasets and case studies from Atapuerca, Spain. Quaternary Geochronology 389, 167-190.

Arnold, L.J., Duval, M., Demuro, M., Spooner, N.A., Santonja, M., Pérez-González, A., 2016. OSL dating of individual quartz ‘supergrains’ from the Ancient Middle Palaeolithic site of Cuesta de la Bajada, Spain. Quaternary Geochronology 36, 78-101.

Arnold, L.J., Demuro, M., Spooner, N.A., Prideaux, G.J., McDowell, M.C., Camens, A.B., Reed, E.H., Parés, J.M., Arsuaga, J.L., Bermúdez de Castro, J.M., Carbonell, E. Single-grain TT-OSL bleaching characteristics: Insights from modern analogues and OSL dating comparisons. Quaternary geochronology, in press (this volume).

Barcos, L., Jabaloy, A., Azdimousa, A., Asebriy, L., Gómez-Ortiz, D., Rodríguez-Peces, M.J., Tejero, R., Pérez-Peña, J.V., 2014. Study of relief changes related to active doming in the eastern Moroccan Rif (Morocco) using geomorphological indices. Journal of African Earth Sciences 100, 493–509.

Bartz, M., Rixhon, G., Duval, M., King, G.E., Álvarez Posada, C., Parés, J.M., Brückner, H., 2018. Successful combination of electron spin resonance, luminescence and palaeomagnetic dating methods allows reconstruction of the Pleistocene evolution of the lower Moulouya river (NE Morocco). Quaternary Science Reviews 185, 153-171.

Brown, N.D., Forman, S.L., 2012. Evaluating a SAR TT-OSL protocol for dating fine-grained quartz within Late Pleistocene loess deposits in the Missouri and Mississippi river valleys, United States. Quaternary Geochronology 12, 87-97.

Demuro, M., Arnold, L.J., Froese, D.G., Roberts, R.G., 2013. OSL dating of loess deposits bracketing Sheep Creek tephra beds, northwest Canada: Dim and problematic single-grain OSL characteristics and their effect on multi-grain age estimates. Quaternary Geochronology 15, 67-87.

Demuro, M., Arnold, L.J., Parés, J.M., Pérez-González, A., Ortega, A.I., Arsuaga, J.L., Bermúdez de Castro, J.M., Carbonell, E., 2014. New luminescence ages for the Galería Complex Archaeological Site: Resolving chronological uncertainties on the Acheulean record of the Sierra de Atapuerca, Northern Spain. PLoS ONE 9 (10), 110-169.

Demuro, M., Arnold, L.J., Parés, J.M., Sala, R., 2015. Extended-range luminescence chronologies suggest potentially complex bone accumulation histories at the Early-to-Middle Pleistocene palaeontological site of Huéscar-1 (Guadix-Baza basin, Spain). Quaternary International 389, 191-212.

Duller, G.A.T., 2003. Distinguishing quartz and feldspar in single grain luminescence measurements. Radiation Measurements 37, 161-165.

Duller, G.A.T., 2012. Improving the accuracy and incision of equivalent doses determined using the optically stimulated luminescence signal from single grains of quartz. Radiation Measurements 47, 770-777.

Duller, G.A.T., Wintle, A.G., 2012. A review of the thermally transferred optically stimulated luminescence signal from quartz for dating sediments. Quaternary Geochronology 7, 6-20.

Durcan, J.A., Duller, G.A.T., 2011. The fast ratio: A rapid measure for testing the dominance of the fast component in the initial OSL signal from quartz. Radiation Measurements 46, 1065-1072.

Galbraith, R.F., Green, P.F., 1990. Estimating the component ages in a finite mixture. Nuclear Tracks and Radiation Measurements 17 (3), 197-206.

Galbraith, R.F., Roberts, R.G., Laslett, G.M., Yoshida, H., Olley, J.M., 1999. Optical dating of single and multiple grains of quartz from Jinmium rock shelter, northern Australia: Part I, experimental design and statistical models. Archaeometry 41 (2), 339-364.

Guérin, G., Murray, A.S., Jain, M., Thomsen, K.J., Mercier, N., 2013. How confident are we in the chronology of the transition between Howieson's Poort and Still Bay? Journal of Human Evolution 64, 314-317.

Jacobs, Z., Roberts, R.G., Lachlan, T.J., Karkanas, P., Marean, C.W., Roberts, D.L., 2011. Development of the SAR TT-OSL procedure for dating Middle Pleistocene dune and shallow marine deposits along the southern Cape coast of South Africa. Quaternary Geochronology 6 (5), 491-513.

Jacobs, Z., Hayes, E.H., Roberts, R.G., Galbraith, R.F., Henshilwood, C.S., 2013. An improved OSL chronology for the Still Bay layers at Blombos cave, South Africa: further tests of single-grain dating procedures and a re-evaluation of the timing of the Still Bay industry across southern Africa. Journal of Archaeological Science 40, 579-594.

Meghraoui, M., Morel, J.-L., Andrieux, J., Dahmani, M., 1996. Tectonique plio-quaternaire de la chaine tello-riffaine et de la mer d'Alboran. Une zone complexe de convergence continent-continent. Bull. Soc. Geol. Fr. 167, 141-157.

Moreno, D., Falguères, C., Pérez-González, A., Duval, M., Voinchet, P., Benito-Calvo, A., Ortega, A.I., Bahain, J.-J., Sala, R., Carbonell, E., Bermúdez de Castro, J.M., Arsuaga, J.L., 2012. ESR chronology of alluvial deposits in the Arlanzón valley (Atapuerca, Spain): Contemporaneity with Atapuerca Gran Dolina site. Quaternary Geochronology 10, 418-423.

Nathan, R.P., Thomas, P.J., Jain, M., Murray, A.S., Rhodes, E.J., 2003. Environmental dose rate heterogeneity of beta radiation and its implications for luminescence dating: Monte Carlo modelling and experimental validation. Radiation Measurements 37, 305-313.

Okoda, M., Suganuma, Y., Henada, Y., Kazaoka, O., 2017. Paleomagnetic direction and paleointensity variations during the Matuyama–Brunhes polarity transition from a marine succession in the Chiba composite section of the Boso Peninsula, central Japan. Earth, Planets and Space 69:45.

Rixhon, G., Bartz, M., El Ouahabi, M., Szemkus, N., Brückner, H., 2017. Contrasting terrace systems of the lower Moulouya river as indicator of crustal deformation in NE Morocco. Journal of African Earth Sciences 126, 45-57.

Stevens, T., Buylaert, J.-P., Murray, A.S., 2009. Towards development of a broadly-applicable SAR TT-OSL dating protocol for quartz. Radiation Measurements 44, 639-645.

Sun, X., Lu, H., Wang, S., Yi, S., Shen, C., Zhang, W., 2013. TT-OSL dating of Longyadong Middle Paleolithic site and palaeoenvironmental implications for hominin occupation in Luonan Basin (central China). Quaternary Research 79, 168-174.

Tsukamoto, S., Duller, G.A.T., Wintle, A.G., 2008. Characteristics of thermally transferred optically stimulated luminescence (TT-OSL) in quartz and its potential for dating sediments. Radiation Measurements 43, 1204-1218.

Wang, X.L., Wintle, A.G., Lu, Y.C., 2006. Thermally transferred luminescence in fine-grained quartz from Chinese loess: Basic observations. Radiation Measurements 41, 649-658.

Yi, S., Lu, H., Stevens, T., 2012. SAR TT-OSL dating of the loess deposits in the Horqin dunefield (northeastern China). Quaternary Geochronology 10, 56-61.

Zielhofer, C., Bussmann, J., Ibouhouten, H., Fenech, K., 2010. Flood frequencies reveal Holocene rapid climate changes (Lower Moulouya River, northeastern Morocco). Journal of Quaternary Science 25, 700-714.

Figure captions

Fig. 1: The study area in NE Morocco (modified after Bartz et al., 2018). a) Relief map of the Moulouya catchment (delimited by dashed black lines) including the main geological structures (according to Barcos et al., 2014); b) The ~20 km-long studied valley reach of the lower Moulouya River with main morphological and geological features as well as the investigated section described in the text (BOU, red star) and investigated by Bartz et al. (2018) (TOLL, MRB and DOE, black stars) (satellite image: Google Earth CNES/Astrium 02.08.2014).

Fig. 2: Chronostratigraphy of the four investigated sections (cf., Bartz et al., 2018). The sections BOU, TOLL and MRB are in the footwall reach and the section DOE in the hanging wall reach of the fault zone (modified after Rixhon et al., 2017 and Bartz et al., 2018). The geochronological framework is based on a combination of ESR of quartz (black), single-grain TT-OSL of quartz (red), $pIRIR_{225}$ of K-feldspar (yellow) and $pIRIR_{290}$ of K-feldspar (green). Palaeomagnetic polarities are shown as black (normal), white (reverse) and grey (inconclusive) bars.

Fig. 3: Representative single-grain TT-OSL decay and dose-response curves for quartz grains from samples C-L3824 and C-L3825. In the insets, the open circle denotes the sensitivity-corrected natural OSL signal, and filled circles denote the sensitivity-corrected regenerated OSL signals. The D_0 value characterises the rate of signal saturation with respect to administered dose and equates to the dose value for which the saturating exponential dose-response curve slope is 1/*e* (or ~ 0.37) of its initial value. (a) Grain from sample C-L3825 with typical OSL signal brightness (T_n intensity = several hundred counts / 0.17 s) and a moderate-to-high Fast Ratio. (b) Grain from sample C-L3824 with a dim TT-OSL signal (T_n intensity <100 counts / 0.17 s), and a moderate-to-high Fast Ratio. (c) Relatively bright grain from sample C-L3825 (T_n intensity = several thousand counts / 0.17 s) with a moderate Fast Ratio. (d) Grain from C-L3824 with typical TT-OSL signal brightness (T_n intensity = several hundred counts / 0.17 s) and a low Fast Ratio.

Fig. 4: Single-grain TT-OSL D_e distributions for samples C-L3824 and C-L3825, shown as radial plots. a) and c) show the D_e datasets obtained for these two samples after applying the routine SAR quality assurance criteria of Arnold et al. (2014); b) and d) show the D_e datasets obtained for the same two samples after applying an additional Fast Ratio acceptance threshold of ≥2 (determined specifically for

each sample using the data shown in Fig. 45). In plot b), the grey band is centred on the weighted mean D_e value used to calculate the TT-OSL ages, which has been determined using the central age model (CAM). In plots a), c) and d), the weighted mean burial dose estimate of the dominant finite mixture model (FMM) component (i.e., that containing the highest proportion of individual D_e values) is shown as a dark grey shaded band on the radial plot. The additional dose components identified by the optimum FMM fits are shown as a light grey shaded band on these radial plots. The percentage of grains associated with each fitted FMM component is also shown on the radial plots.

Fig. 5: Relationship between single-grain TT-OSL D_e estimates and Fast Ratios for samples C-L3824 and C-L3825. a) RegressionX-Y plot of TT-OSL D_e versus Fast Ratio for individual grains of C-L3824 and C-L3825; b) Plot showing the weighted mean (CAM) D_e and overdispersion values obtained for C-L3824 when applying different Fast Ratio thresholds; c) Plot showing the weighted mean (CAM) D_e and overdispersion values obtained for C-L3825 when applying different Fast Ratio thresholds. In plots b) and c), progressively higher Fast Ratio thresholds have been applied to the D_e dataset, starting at a Fast Ratio of 0 and increasing in Fast Ratio increments of 0.5 until the culled dataset contained fewer than 10 individual D_e values (i.e., the sample size became too limited to ensure precise single-grain D_e determination). In each instance, grains were only accepted for further D_e analysis if their individual Fast Ratio value equalled or exceeded the corresponding threshold shown on the x-axis. The values shown in brackets represent the number of grains remaining in the D_e dataset after applying each Fast Ratio threshold criterion.

Table captions

Tab. 1: Summary of the single-grain TT-OSL dating results obtained in the present work. Details can be found in supplementary material. ESR and pIRIR ages are also provided for comparison of all samples (C-L3824-3826) from the BOU section (cf., Bartz et al., 2018).

Single-grain TT-OSL dating results confirm an Early Pleistocene age for the lower Moulouya River deposits (NE Morocco)

M. Bartz[1*], L.J. Arnold[2], M. Demuro[2], M. Duval[3], G.E. King[4], G. Rixhon[5], C. Álvarez Posada[6], J.M. Parés[6] and H. Brückner[1]

[1] Institute of Geography, University of Cologne, Albertus-Magnus-Platz, 50923 Cologne/Germany

[2] School of Physical Sciences, Environment Institute, and Institute for Photonics and Advanced Sensing (IPAS), University of Adelaide, North Terrace Campus, Adelaide, SA, 5005/Australia

[3] Australian Research Centre for Human Evolution (ARCHE), Environmental Futures Research Institute (EFRI), Griffith University, 170 Kessels Road, Nathan, QLD 4111/Australia

[4] Institute of Geological Sciences, University of Bern, Baltzerstr. 1-3, 3012 Bern/Switzerland

[5] Laboratoire Image, Ville, Environnement (LIVE), UMR 7362 - CNRS, University of Strasbourg-ENGEES, 3 rue de l'Argonne, 67083 Strasbourg Cedex/France

[6] Centro Nacional de Investigación sobre la Evolución Humana (CENIEH), Paseo de Atapuerca, s/n, 09002 Burgos/Spain

*corresponding author: m.bartz@uni-koeln.de; +492214707719

Abstract

The lower Moulouya River (NE Morocco) drains a tectonically active area related to the NW-SE convergence of the African and Eurasian plates. Fluvial deposits preserved in the lower Moulouya have been dated to ~1.5-1.1 Ma as part of a recent multi-technique geochronology study. The present work aims to verify and refine the existing Early Pleistocene (~1.8-0.8 Ma) ages for the Moulouya deposits using single-grain thermally transferred-OSL (TT-OSL) dating. The single-grain TT-OSL D_e distributions are characterised by high overdispersion (77-91 %), significant negative skewness, and several discrete populations can be identified when applying the finite mixture model (FMM). The lowest FMM dose components of the TT-OSL datasets comprise relatively dim grains that have very slow decays. The Fast Ratio (FR) was therefore used to explore whether the presence of slower-decaying TT-OSL components might have exerted a significant effect on our D_e values. Our samples show a 40-50 % increase in weighted mean D_e and a 50-100 % decrease in overdispersion when applying a FR acceptance threshold of 2, resulting in the elimination of the lowest FMM component. Application of a higher FR value does not result in any additional change in TT-OSL D_e value. Dose recovery tests confirm the suitability of the single-grain TT-OSL protocol and use of an additional FR acceptance threshold of ≥2 for final age determination. Previous geomorphic interpretations suggested a capture event occurred at the Beni Snassen gorge between 1.04 and 1.36 Ma at the latest. This interpretation is supported by the newly obtained TT-OSL ages, which reveal that fluvial deposition occurred between ~1.09 and ~1.15 Ma.

Keywords: Quartz, single-grain, TT-OSL, fluvial terraces, Morocco

1. Introduction

The Moulouya River (~74.000 km^2; Fig. 1a), drains an active tectonic setting resulting from the collision between the Eurasian and African plates, which leads to a complex geodynamic background in this convergence zone (Meghraoui et al., 1996; Barcos et al., 2014). Along the ~600 km-long Moulouya drainage, the sedimentary infill (including Quaternary fluvial deposits) of the lowermost Neogene basin (the so-called Triffa basin) is thus strongly deformed along a sub-continuous W-E striking thrust zone (Rixhon et al., 2017; Fig. 1b). As for the geochronology of the lower Moulouya, in addition to ^{14}C dating of the Holocene sedimentary record (e.g., Zielhofer et al., 2010), a recent study based on a combination of electron spin resonance (ESR) dating of quartz using the multiple centres (MC) approach, post-infrared infrared (pIRIR) stimulated luminescence dating of K-feldspar, and magnetostratigraphy has yielded a reliable framework for the Pleistocene terrace deposits (Bartz et al., 2018). ESR numerical ages, all clustering between ~1.1 and 1.5 Ma, are supported by a reversed polarity in almost all river profiles; the presumed absence of Middle Pleistocene river sediments in the Triffa basin seems to rule out climate as the main driver for fluvial deposition (Bartz et al., 2018).

Against this background, the present study aims to verify and refine the existing chronostratigraphy of the lower Moulouya using single-grain thermally transferred-OSL (TT-OSL) dating. TT-OSL dating (Wang et al., 2006) makes use of a quartz luminescence signal that saturates at much higher radiation doses than the conventional OSL signal. In sedimentary archives, the TT-OSL signal has mostly been applied to aeolian (e.g., Stevens et al., 2009; Yi et al., 2012), marine (e.g., Jacobs et al., 2011) and archaeological (e.g., Sun et al., 2013; Demuro et al., 2014; Arnold et al., 2015) deposits spanning Early and Middle Pleistocene timescales. Nevertheless, establishing reliable TT-OSL chronologies over such 'extended' age ranges has often proved challenging due to a number of complications with multi-grain TT-OSL signal characteristics (e.g., signal sensitivity, bleachability, thermal stability; Duller and Wintle, 2012).

Recently, single-grain TT-OSL dating has been reliably applied to several independently or semi-independently dated sedimentary archives (e.g., Arnold et al., 2014; Demuro et al., 2015). For samples with sufficiently bright signals, single-grain TT-OSL offers a number of potential advantages over multi-grain TT-OSL approaches; particularly the ability to isolate grains with favourable TT-OSL properties, the detection of inter-grain differences in problematic TT-OSL behaviours (including low thermal stabilities), and a means of circumventing averaging effects arising from simultaneously measuring grains with different bleaching histories, signal compositions or TT-OSL source trap properties (Arnold et al., 2014; Arnold and Demuro et al., 2015; Arnold et al., this volume). In the fluvial context, Arnold et al. (2013) compared the suitability of both single-grain and multi-grain TT-OSL dating on deposits from the Pico River in northern Spain, obtaining consistent ages of ~350 and ~330 ka, respectively. These TT-OSL ages were in agreement with ESR quartz ages, based on the aluminium centre, from adjacent river terraces (Moreno et al., 2012). Single-grain TT-OSL therefore offers a potentially viable means of dating the Moulouya quartz samples and may help further understand the Early Pleistocene depositional history.

2. Sampling and luminescence dating procedures

Four >20 m-thick fluvial sections were investigated by Bartz et al. (2018) in the Triffa basin, the so-called BOU, DOE, MRB and TOLL profiles (see Figs. 1b and 2). The initial geochronological framework was based on the MC approach in ESR dating, which involved measuring both the Al and Ti centres in each quartz sample (Fig. 2). The ages obtained using this approach were consistent with reversed magnetic polarities found in the fluvial deposits (Bartz et al., 2018), and revealed that fluvial aggradation took place between ~1.5 and ~1.1 Ma (Fig. 2). In addition, post-infrared infrared (pIRIR) stimulated luminescence measurements undertaken as part of the same study showed that both the $pIRIR_{225}$ and $pIRIR_{290}$ signals were saturated, yielding minimum ages between ~0.39 and ~0.80 Ma (Bartz et al., 2018).

In this study, two samples from the BOU section (C-L3824 and C-L3825) were investigated to test the applicability of single-grain TT-OSL (Fig. 2), which may yield non-saturated signals over these timescales and thus may provide further numerical age constraint on fluvial deposition in the Moulouya basin.

Sample preparation for luminescence dating was undertaken at the Cologne Luminescence Laboratory (CLL), University of Cologne. Single-grain TT-OSL measurements (Arnold et al., 2014) were made at the Prescott Environmental Luminescence Laboratory, University of Adelaide. Full details of the sample preparation, measurement equipment and protocol (Tab. S1), as well as the laboratory experiments employed in this study, are provided in the supplementary material. Radionuclide data and dose rates (Tab. S2) for all samples are presented in supplementary material.

The equivalent dose (D_e) quality assurance criteria used as part of the single-grain TT-OSL dating procedures followed Arnold et al. (2014). Grains were rejected from consideration if they displayed: (i) T_n <3σ background; (ii) Recycling ratio ≠ 1 at ±2σ; (iii) 0 Gy L_x/T_x >5% L_n/T_n ; (iv) OSL-IR depletion ratios <1 at ±2σ (Duller, 2003); (v) Non-intersecting grains (L_n/T_n > dose response curve saturation); (vi) Saturated grains ($L_n/T_n \geq$ dose response curve I_{max} at ±2σ); (vii) Extrapolated grains (L_n/T_n > highest L_x/T_x at ±2σ) and (viii) Anomalous dose response / unable to perform Monte Carlo fit.

The Fast Ratio (FR) (Durcan and Duller, 2011; Duller, 2012) has been applied to the two BOU samples to provide a proxy for TT-OSL charge transfer into the fast OSL component trap relative to the medium and slow OSL component traps, as well as for identifying the dominance of potentially interfering (non-transferred) residual slow OSL components in the TT-OSL signals (see Supplementary material). The FR has been calculated by comparing the counts in the initial part of the TT-OSL decay curve (L_1) with those in the middle part of the decay (L_2) after subtracting a late light background count (L_3) according to the equation $(L_1\text{-}L_3)/(L_2\text{-}L_3)$. The FRs for our single-grain D_e datasets were calculated using the approach described in Duller (2012), but with the integration intervals specified by Jacobs et al. (2013) (i.e., the first 0.017 s for the L_1, 0.170-0.221 s for L_2 and the last 0.068 s for L_3), since these are based on the 90 % laser power used in the present study. Progressively higher FR thresholds have been applied to the single-grain TT-OSL D_e datasets, starting at a FR of 0 and increasing in FR increments of 0.5 until the culled dataset contained fewer than 10 individual D_e values (i.e., the sample size became too limited to ensure precise single-grain D_e determination). In each instance, grains were only accepted for further D_e analysis if their individual FR value equalled or exceeded the corresponding FR threshold.

A single-grain TT-OSL dose-recovery test was performed on a batch of 1000 unbleached grains of sample C-L3824 owing to the long durations of light exposure needed to bleach natural TT-OSL signals down to low residual levels (e.g., Demuro et al., 2015; Arnold et al., this volume). A known (941 Gy) laboratory dose of similar magnitude to the expected D_e was added on top of the natural signal for these grains. The expected D_e was initially determined by undertaking a sub-set of natural D_e measurements on 300 grains of sample C-L3824 prior to performing the dose-recovery test. The recovered dose was calculated by subtracting the weighted mean natural D_e of sample C-L3824 (i.e., as shown in Table 1 determined from 1600 grains) from the weighted mean D_e of the unbleached and dosed grains.

3. Results and discussion

3.1 Single-grain TT-OSL properties and dose distributions

Between 1000 and 1600 single-grain TT-OSL D_e measurements were made on samples C-L3824 and C-L3825. Application of the SAR quality assurance criteria of Arnold et al. (2014) resulted in 2–4 % of measured D_e values being accepted for age calculation (Tab. S3). The vast majority of remaining D_e values (86-88 %) were eliminated for having very weak T_n signals (<3σ background), with smaller populations rejected for having poor recycling ratios that were not consistent with unity at 2σ (3 %) and anomalous/scattered dose-responses that could not be fitted with the Monte Carlo procedure (7 %). The TT-OSL decay curves of accepted grains have relatively low T_n intensities of 50–2000 cts/0.17 s, and the corresponding dose response curves are generally well represented by a single saturating exponential fitting function with D_0 values of 10^2-10^3 Gy (Fig. 3).

The single-grain TT-OSL D_e distributions (Fig. 4) are characterised by high overdispersion values of 77-91 % (Tab. S4), which are well above the average reported value for 'ideal' single-grain TT-OSL samples (21±2 %; Arnold et al., this volume). Both D_e distributions are significantly negatively skewed according to the criteria outlined by Arnold and Roberts (2009) (Tab. S4), and both datasets contain several discrete dose populations when fitted with the finite mixture model (FMM; Galbraith and Green, 1990) (Fig. 4a, c). The dominant FMM components (i.e., those containing the highest proportion of individual D_e values; n = 34 and 27 grains for C-L3824 and C-L3825, respectively) yield ages in agreement with the ESR dating estimates of ~1.1-1.3 Ma for BOU (Bartz et al., 2018) (Fig. 2). However, the lower dose FMM components underestimate the existing site chronology by 68-96 % (Tab. S4). Similar low dose components were observed in the Early Pleistocene single-grain TT-OSL study of Arnold and Demuro (2015), and were attributed to inter-grain variations in TT-OSL signal characteristics. Given the well-stratified nature of these fluvial deposits, it seems unlikely that post-depositional mixing could explain the multi-modal D_e distributions of samples C-L3824 and C-L3825.

Similarly, beta dose heterogeneity is unlikely to give rise to such extreme and discrete low dose components in most typical sedimentary contexts (e.g., Nathan et al., 2003; Guérin et al., 2013). It seems possible therefore, that intrinsic sources of D_e scatter may partly or wholly explain these complex single-grain TT-OSL datasets.

Several of the accepted grains from samples C-L3824 and C-L3825 display very slowly decaying TT-OSL signals (i.e., T_x signals that did not reach background after 2 s of laser stimulation) (e.g., Fig. 3d). Such slow-decay dominated signals have been shown to be associated with potentially problematic TT-OSL behaviours (poor dose recovery test results, inferior thermal stabilities, experimentally sensitised components and unreliable TT-OSL D_e estimates) for some samples (e.g., Tsukamoto et al., 2008; Brown and Forman, 2012; Arnold and Demuro, 2015; Demuro et al., 2015). It may therefore be appropriate to introduce an additional signal quality assurance criterion to remove these slowly decaying signals, which we explore in the following sections.

3.2 Application of single-grain Fast Ratios (FR)

To examine whether TT-OSL charge transfer into slowly bleaching OSL traps or the presence of interfering (non-transferred) slow OSL signal components might have exerted a significant effect on our D_e datasets, we calculated single-grain Fast Ratios (FR) (Durcan and Duller, 2011; Duller, 2012) using the approach described in Demuro et al. (2013). Although TT-OSL signals are thermally transferred from a different source trap into the conventional OSL dating trap, any unfavourable behaviour associated with the latter (i.e., medium or slow component dominance, and hence low FR value) or interference from additional (non-conventional) OSL traps may be indicative of potentially unsuitable quartz behaviour.

The range of FRs obtained for our TT-OSL datasets (0.2–54) are lower than those reported for single-grain OSL datasets (e.g., 1.1–108 in Demuro et al., 2013). The lowest individual D_e values (<300 Gy) in both datasets yield correspondingly low FR values (Fig. 5a). In order to examine the potential of using the FR as an additional rejection criterion for single-grain data analysis, we applied increasingly stringent FR thresholds to the accepted D_e datasets, and examined the effects on weighted mean D_e and overdispersion (Fig. 5b-c). Both samples show a 40-50 % increase in weighted mean D_e and a 50-100

% decrease in overdispersion when applying incrementally higher FR acceptance thresholds between 0 and 2. Use of more stringent FR acceptance ratios >2 has no further discernible effect on D_e or overdispersion, other than causing a fourfold reduction in the number of accepted grains (Fig. 5b-c). These results suggest that slow decaying TT-OSL grains with FRs <2 exert an influence on the single-grain TT-OSL datasets. It may therefore be beneficial to employ an additional SAR quality assurance criterion based on a FR threshold of ≥2 for these samples. This is supported by the resultant D_e distribution characteristics and FMM fitting results shown in Fig. 4b, d. Application of a FR acceptance threshold of ≥2 results in the elimination of the lowest FMM component for both samples. The revised D_e distribution of C-L3824 is no longer considered to be significantly negatively skewed, has an overdispersion of 0 %, and is well represented by a single dose population centred on the central age model (CAM) D_e value (Galbraith et al., 1999; Tab. S4). The initially identified low dose FMM component for this sample therefore seemingly originated from grains with slowly decaying TT-OSL signals that are poorly suited to being measured with a SAR protocol. The revised D_e distribution of C-L3825 retains one of the two originally identified low dose FMM components and is still considered to be negatively skewed. However, its overdispersion is reduced by 50 % and the dominant FMM component now accounts for a significant proportion (~80 %) of measured grains (Tab. S4). The latter has therefore been used to derive the final age for this sample. The minor low dose FMM component remaining after applying the FR ≥2 acceptance threshold potentially originates from other sources of intrinsic D_e scatter (e.g., fast-dominated grains that do not respond well to the SAR conditions or grains with thermally unstable TT-OSL signals) or unidentified extrinsic D_e scatter. As with sample C-L3824, it seems that the initially identified FMM K_1 dose component originated from grains with slowly decaying TT-OSL signals.

3.3 Dose recovery results

A TT-OSL dose recovery test performed on C-L3824 (Fig. S1) attests to the general suitability of the single-grain TT-OSL protocol and use of an additional FR acceptance threshold of ≥2 for final age determination. The FR characteristics and D_e distribution of the unbleached and dosed grains mirror those obtained for the natural D_e dataset of C-L3824 (Fig. S1). The low dose FFM component observed for the unbleached and dosed dataset also lies significantly below the administered dose of 941 Gy, confirming an intrinsic rather than extrinsic origin for the D_e scatter. A net (i.e., natural-subtracted) recovered-to-given ratio of 1.04±0.07 and an overdispersion value of 0 % was obtained for the unbleached and dosed grains of this sample when applying a FR acceptance threshold of ≥2.

3.4 Consolidating the chronostratigraphy for the Lower Moulouya fluvial terraces

The single-grain TT-OSL ages obtained for the uppermost part of the BOU section are stratigraphically consistent: the lowermost sample (C-L3824) yielded an age of 1.09±0.10 Ma, while the upper sample (C-L3825) provided an age of 1.15±0.10 Ma (Fig. 2). The two new numerical ages are consistent at 1σ with the corresponding ESR ages of 1.26±0.10 and 1.10±0.11 Ma (Tab.1) derived from the same samples, and the reversed magnetic polarities identified at this section (Bartz et al., 2018). When combined with the existing ESR ages and magnetostratigraphy, the new TT-OSL data provide a refined chronological framework for the evolution of the Moulouya terraces during the Early Pleistocene. Collectively, the former and new numerical age estimates unequivocally point to the occurrence of a major depositional event in the lowermost sedimentary basin during the Matuyama chron (>0.77 Ma; Okoda et al., 2017). The chronologies developed in this study strongly supports many of the geomorphological interpretations previously reached by Bartz et al. (2018). In particular, they confirm the time span over which the assumed capture event took place through the uplifting Beni Snassen (i.e., linking the Guercif and Triffa basins via the Beni Snassen gorge; Bartz et al., 2018); that is between 1.05 and 1.25 Ma at the latest (according to the TT-OSL age provided by the upper sample C-L3825). They also demonstrate the usefulness of cross-checking ages obtained from independent dating methods to establish a particularly robust chronological framework for reconstructing long-term landscape evolution.

3.5 Reliability of the single-grain TT-OSL ages

In assessing the reliability of the final single-grain TT-OSL ages, it is worth briefly considering two issues: (i) the slow optical resetting rates of TT-OSL signals and the potential retention of unbleached residuals prior to deposition; (ii) the possible need for applying a thermal stability correction when applying TT-OSL signal over extended burial periods. The recent modern analogue study by Arnold et al. (this volume) revealed single-grain TT-OSL residual doses of 0-24 Gy for comparable dryland fluvial deposits from Spain and Australia. Such residual D_e values would be largely insignificant over the burial dose ranges considered here, and would be well within the existing 2σ TT-OSL D_e uncertainties for samples C-L3824 and C-L3825. Reported lifetime estimates for TT-OSL signals are highly variable (e.g., Adamiec et al., 2010; Brown and Forman, 2012) and have been exclusively derived using multi-grain TL loss and isothermal decay datasets. Arnold and Demuro (2015) have shown that multi-grain assessments of TL signal loss may provide limited insights into single-grain TT-OSL source trap lifetimes due to averaging effects, the dominance of grain populations that do not produce TT-OSL, and interference from slowly bleaching OSL components. As we cannot be confident that existing (multi-grain aliquot) laboratory lifetime predictions are of direct relevance to the specific grain populations isolated in our single-grain analysis, we have not applied an additional thermal stability correction to the final TT-OSL ages. This decision appears to be supported by the consistency of the single-grain TT-OSL and ESR ages at BOU (cf., Bartz et al., 2018), which suggests that any potential age underestimations related to thermal instability are not significant beyond the existing uncertainty ranges of our final chronologies.

4. Conclusion

The existing geochronological framework for the lower Moulouya terraces, which is based on a combination of ESR, pIRIR and palaeomagnetism (cf., Bartz et al., 2018), has been successfully verified by quartz single-grain TT-OSL dating in this study. The consistency between the newly obtained single-grain TT-OSL ages and the existing ESR and palaeomagnetism chronologies is particularly encouraging, and it indicates that massive fluvial deposition occurred in the lower Moulouya towards the end of the Early Pleistocene. Whilst application of conventional OSL and pIRIR dating remains unsuccessful over Early Pleistocene timescales due to signal saturation, our results show that single-grain TT-OSL can successfully be applied over extended age ranges in some settings. The TT-OSL ages presented in this study are the oldest published so far and their reliability is supported by independent dating evidence. Importantly, suitable D_e determination was only achievable for these samples after undertaking grain-specific assessments of TT-OSL signal variability, and applying an additional quality assurance criterion based on a FR acceptance threshold of ≥2. This may not have been possible, at least to the same extent, if we had employed conventional, multi-grain TT-OSL dating on these fluvial deposits.

Acknowledgements

This project is affiliated to the CRC 806 “Our Way to Europe”, which is generously funded by the German Research Foundation [DFG; Grant-No.: SFB 806/2]. The support by the “Institut National des Sciences de l’Archéologie et du Patrimoine du Maroc” (INSAP) and by the “Commission for Archaeology of Non-European Cultures” (KAAK) of the German Archaeological Institute (DAI) is gratefully acknowledged, in particular of Abdeslam Mikdad and Josef Eiwanger, respectively. Aspects of the study have been funded by Australian Research Council Grant FT130100195 awarded to Lee J. Arnold, FT150100215 awarded to Mathieu Duval and DE160100743 awarded to Martina Demuro. Georgina E. King acknowledges support from Swiss National Science Foundation grant number PZ00P2-167960.

References

Adamiec, G., Duller, G.A.T., Roberts, H.M., Wintle, A.G., 2010. Improving the TT-OSL SAR protocol through source trap characterisation. Radiation Measurements 45, 768-777.

Arnold, L.J., Roberts, R.G., 2009. Stochastic modelling of multi-grain equivalent dose (D_e) distributions: Implications for OSL dating of sediment mixtures. Quaternary Geochronology 4, 204-230.

Arnold, L.J., Demuro, M., Navazo, M., Benito-Calvo, A., Pérez-González, A., 2013. OSL dating of the Middle Palaeolithic Hotel California site, Sierra de Atapuerca, north-central Spain. Boreas 42, 285-305.

Arnold, L.J., Demuro, M., Parés, J.M., Arsuaga, J.L., Aranburu, A., Bermudéz de Castro, J.M., Carbonell, E., 2014. Luminescence dating and palaeomagnetic age constraint on hominins from Sima de los Huesos, Atapuerca, Spain. Journal of Human Evolution 67, 85-107.

Arnold, L.J., Demuro, M., 2015. Insights into TT-OSL signal stability from single-grain analyses of known-age deposits at Atapuerca, Spain. Quaternary Geochronology 30, 472-478.

Arnold, L.J., Demuro, M., Parés, J.M., Pérez-González, A., Arsuaga, J.L., Bermúdez de Castro, J.M., Carbonell, E., 2015. Evaluating the suitability of extended-range luminescence dating techniques over early and Middle Pleistocene timescales: Published datasets and case studies from Atapuerca, Spain. Quaternary Geochronology 389, 167-190.

Arnold, L.J., Duval, M., Demuro, M., Spooner, N.A., Santonja, M., Pérez-González, A., 2016. OSL dating of individual quartz ‘supergrains’ from the Ancient Middle Palaeolithic site of Cuesta de la Bajada, Spain. Quaternary Geochronology 36, 78-101.

Arnold, L.J., Demuro, M., Spooner, N.A., Prideaux, G.J., McDowell, M.C., Camens, A.B., Reed, E.H., Parés, J.M., Arsuaga, J.L., Bermúdez de Castro, J.M., Carbonell, E. Single-grain TT-OSL bleaching characteristics: Insights from modern analogues and OSL dating comparisons. Quaternary geochronology, in press (this volume).

Barcos, L., Jabaloy, A., Azdimousa, A., Asebriy, L., Gómez-Ortiz, D., Rodríguez-Peces, M.J., Tejero, R., Pérez-Peña, J.V., 2014. Study of relief changes related to active doming in the eastern Moroccan Rif (Morocco) using geomorphological indices. Journal of African Earth Sciences 100, 493–509.

Bartz, M., Rixhon, G., Duval, M., King, G.E., Álvarez Posada, C., Parés, J.M., Brückner, H., 2018. Successful combination of electron spin resonance, luminescence and palaeomagnetic dating methods allows reconstruction of the Pleistocene evolution of the lower Moulouya river (NE Morocco). Quaternary Science Reviews 185, 153-171.

Brown, N.D., Forman, S.L., 2012. Evaluating a SAR TT-OSL protocol for dating fine-grained quartz within Late Pleistocene loess deposits in the Missouri and Mississippi river valleys, United States. Quaternary Geochronology 12, 87-97.

Demuro, M., Arnold, L.J., Froese, D.G., Roberts, R.G., 2013. OSL dating of loess deposits bracketing Sheep Creek tephra beds, northwest Canada: Dim and problematic single-grain OSL characteristics and their effect on multi-grain age estimates. Quaternary Geochronology 15, 67-87.

Demuro, M., Arnold, L.J., Parés, J.M., Pérez-González, A., Ortega, A.I., Arsuaga, J.L., Bermúdez de Castro, J.M., Carbonell, E., 2014. New luminescence ages for the Galería Complex Archaeological Site: Resolving chronological uncertainties on the Acheulean record of the Sierra de Atapuerca, Northern Spain. PLoS ONE 9 (10), 110-169.

Demuro, M., Arnold, L.J., Parés, J.M., Sala, R., 2015. Extended-range luminescence chronologies suggest potentially complex bone accumulation histories at the Early-to-Middle Pleistocene palaeontological site of Huéscar-1 (Guadix-Baza basin, Spain). Quaternary International 389, 191-212.

Duller, G.A.T., 2003. Distinguishing quartz and feldspar in single grain luminescence measurements. Radiation Measurements 37, 161-165.

Duller, G.A.T., 2012. Improving the accuracy and incision of equivalent doses determined using the optically stimulated luminescence signal from single grains of quartz. Radiation Measurements 47, 770-777.

Duller, G.A.T., Wintle, A.G., 2012. A review of the thermally transferred optically stimulated luminescence signal from quartz for dating sediments. Quaternary Geochronology 7, 6-20.

Durcan, J.A., Duller, G.A.T., 2011. The fast ratio: A rapid measure for testing the dominance of the fast component in the initial OSL signal from quartz. Radiation Measurements 46, 1065-1072.

Galbraith, R.F., Green, P.F., 1990. Estimating the component ages in a finite mixture. Nuclear Tracks and Radiation Measurements 17 (3), 197-206.

Galbraith, R.F., Roberts, R.G., Laslett, G.M., Yoshida, H., Olley, J.M., 1999. Optical dating of single and multiple grains of quartz from Jinmium rock shelter, northern Australia: Part I, experimental design and statistical models. Archaeometry 41 (2), 339-364.

Guérin, G., Murray, A.S., Jain, M., Thomsen, K.J., Mercier, N., 2013. How confident are we in the chronology of the transition between Howieson's Poort and Still Bay? Journal of Human Evolution 64, 314-317.

Jacobs, Z., Roberts, R.G., Lachlan, T.J., Karkanas, P., Marean, C.W., Roberts, D.L., 2011. Development of the SAR TT-OSL procedure for dating Middle Pleistocene dune and shallow marine deposits along the southern Cape coast of South Africa. Quaternary Geochronology 6 (5), 491-513.

Jacobs, Z., Hayes, E.H., Roberts, R.G., Galbraith, R.F., Henshilwood, C.S., 2013. An improved OSL chronology for the Still Bay layers at Blombos cave, South Africa: further tests of single-grain dating procedures and a re-evaluation of the timing of the Still Bay industry across southern Africa. Journal of Archaeological Science 40, 579-594.

Meghraoui, M., Morel, J.-L., Andrieux, J., Dahmani, M., 1996. Tectonique plio-quaternaire de la chaine tello-riffaine et de la mer d'Alboran. Une zone complexe de convergence continent-continent. Bull. Soc. Geol. Fr. 167, 141-157.

Moreno, D., Falguères, C., Pérez-González, A., Duval, M., Voinchet, P., Benito-Calvo, A., Ortega, A.I., Bahain, J.-J., Sala, R., Carbonell, E., Bermúdez de Castro, J.M., Arsuaga, J.L., 2012. ESR chronology of alluvial deposits in the Arlanzón valley (Atapuerca, Spain): Contemporaneity with Atapuerca Gran Dolina site. Quaternary Geochronology 10, 418-423.

Nathan, R.P., Thomas, P.J., Jain, M., Murray, A.S., Rhodes, E.J., 2003. Environmental dose rate heterogeneity of beta radiation and its implications for luminescence dating: Monte Carlo modelling and experimental validation. Radiation Measurements 37, 305-313.

Okoda, M., Suganuma, Y., Henada, Y., Kazaoka, O., 2017. Paleomagnetic direction and paleointensity variations during the Matuyama–Brunhes polarity transition from a marine succession in the Chiba composite section of the Boso Peninsula, central Japan. Earth, Planets and Space 69:45.

Rixhon, G., Bartz, M., El Ouahabi, M., Szemkus, N., Brückner, H., 2017. Contrasting terrace systems of the lower Moulouya river as indicator of crustal deformation in NE Morocco. Journal of African Earth Sciences 126, 45-57.

Stevens, T., Buylaert, J.-P., Murray, A.S., 2009. Towards development of a broadly-applicable SAR TT-OSL dating protocol for quartz. Radiation Measurements 44, 639-645.

Sun, X., Lu, H., Wang, S., Yi, S., Shen, C., Zhang, W., 2013. TT-OSL dating of Longyadong Middle Paleolithic site and palaeoenvironmental implications for hominin occupation in Luonan Basin (central China). Quaternary Research 79, 168-174.

Tsukamoto, S., Duller, G.A.T., Wintle, A.G., 2008. Characteristics of thermally transferred optically stimulated luminescence (TT-OSL) in quartz and its potential for dating sediments. Radiation Measurements 43, 1204-1218.

Wang, X.L., Wintle, A.G., Lu, Y.C., 2006. Thermally transferred luminescence in fine-grained quartz from Chinese loess: Basic observations. Radiation Measurements 41, 649-658.

Yi, S., Lu, H., Stevens, T., 2012. SAR TT-OSL dating of the loess deposits in the Horqin dunefield (northeastern China). Quaternary Geochronology 10, 56-61.

Zielhofer, C., Bussmann, J., Ibouhouten, H., Fenech, K., 2010. Flood frequencies reveal Holocene rapid climate changes (Lower Moulouya River, northeastern Morocco). Journal of Quaternary Science 25, 700-714.

Figure captions

Fig. 1: The study area in NE Morocco (modified after Bartz et al., 2018). a) Relief map of the Moulouya catchment (delimited by dashed black lines) including the main geological structures (according to Barcos et al., 2014); b) The ~20 km-long studied valley reach of the lower Moulouya River with main

morphological and geological features as well as the investigated section described in the text (BOU, red star) and investigated by Bartz et al. (2018) (TOLL, MRB and DOE, black stars) (satellite image: Google Earth CNES/Astrium 02.08.2014).

Fig. 2: Chronostratigraphy of the four investigated sections (cf., Bartz et al., 2018). The sections BOU, TOLL and MRB are in the footwall reach and the section DOE in the hanging wall reach of the fault zone (modified after Rixhon et al., 2017 and Bartz et al., 2018). The geochronological framework is based on a combination of ESR of quartz (black), single-grain TT-OSL of quartz (red), $pIRIR_{225}$ of K-feldspar (yellow) and $pIRIR_{290}$ of K-feldspar (green). Palaeomagnetic polarities are shown as black (normal), white (reverse) and grey (inconclusive) bars.

Fig. 3: Representative single-grain TT-OSL decay and dose-response curves for quartz grains from samples C-L3824 and C-L3825. In the insets, the open circle denotes the sensitivity-corrected natural OSL signal, and filled circles denote the sensitivity-corrected regenerated OSL signals. The D_0 value characterises the rate of signal saturation with respect to administered dose and equates to the dose value for which the saturating exponential dose-response curve slope is 1/*e* (or ~ 0.37) of its initial value. (a) Grain from sample C-L3825 with typical OSL signal brightness (T_n intensity = several hundred counts / 0.17 s) and a moderate-to-high Fast Ratio. (b) Grain from sample C-L3824 with a dim TT-OSL signal (T_n intensity <100 counts / 0.17 s), and a moderate-to-high Fast Ratio. (c) Relatively bright grain from sample C-L3825 (T_n intensity = several thousand counts / 0.17 s) with a moderate Fast Ratio. (d) Grain from C-L3824 with typical TT-OSL signal brightness (T_n intensity = several hundred counts / 0.17 s) and a low Fast Ratio.

Fig. 4: Single-grain TT-OSL D_e distributions for samples C-L3824 and C-L3825, shown as radial plots. a) and c) show the D_e datasets obtained for these two samples after applying the routine SAR quality assurance criteria of Arnold et al. (2014); b) and d) show the D_e datasets obtained for the same two samples after applying an additional Fast Ratio acceptance threshold of ≥2 (determined specifically for each sample using the data shown in Fig. 5). In plot b), the grey band is centred on the weighted mean D_e value used to calculate the TT-OSL ages, which has been determined using the central age model (CAM). In plots a), c) and d), the weighted mean burial dose estimate of the dominant finite mixture

model (FMM) component (i.e., that containing the highest proportion of individual D_e values) is shown as a dark grey shaded band on the radial plot. The additional dose components identified by the optimum FMM fits are shown as a light grey shaded band on these radial plots. The percentage of grains associated with each fitted FMM component is also shown on the radial plots.

Fig. 5: Relationship between single-grain TT-OSL D_e estimates and Fast Ratios for samples C-L3824 and C-L3825. a) X-Y plot of TT-OSL D_e versus Fast Ratio for individual grains of C-L3824 and C-L3825; b) Plot showing the weighted mean (CAM) D_e and overdispersion values obtained for C-L3824 when applying different Fast Ratio thresholds; c) Plot showing the weighted mean (CAM) D_e and overdispersion values obtained for C-L3825 when applying different Fast Ratio thresholds. In plots b) and c), progressively higher Fast Ratio thresholds have been applied to the D_e dataset, starting at a Fast Ratio of 0 and increasing in Fast Ratio increments of 0.5 until the culled dataset contained fewer than 10 individual D_e values (i.e., the sample size became too limited to ensure precise single-grain D_e determination). In each instance, grains were only accepted for further D_e analysis if their individual Fast Ratio value equalled or exceeded the corresponding threshold shown on the x-axis. The values shown in brackets represent the number of grains remaining in the D_e dataset after applying each Fast Ratio threshold criterion.

Table captions

Tab. 1: Summary of the single-grain TT-OSL dating results obtained in the present work. Details can be found in supplementary material. ESR and pIRIR ages are also provided for comparison of all samples (C-L3824-3826) from the BOU section (cf., Bartz et al., 2018).

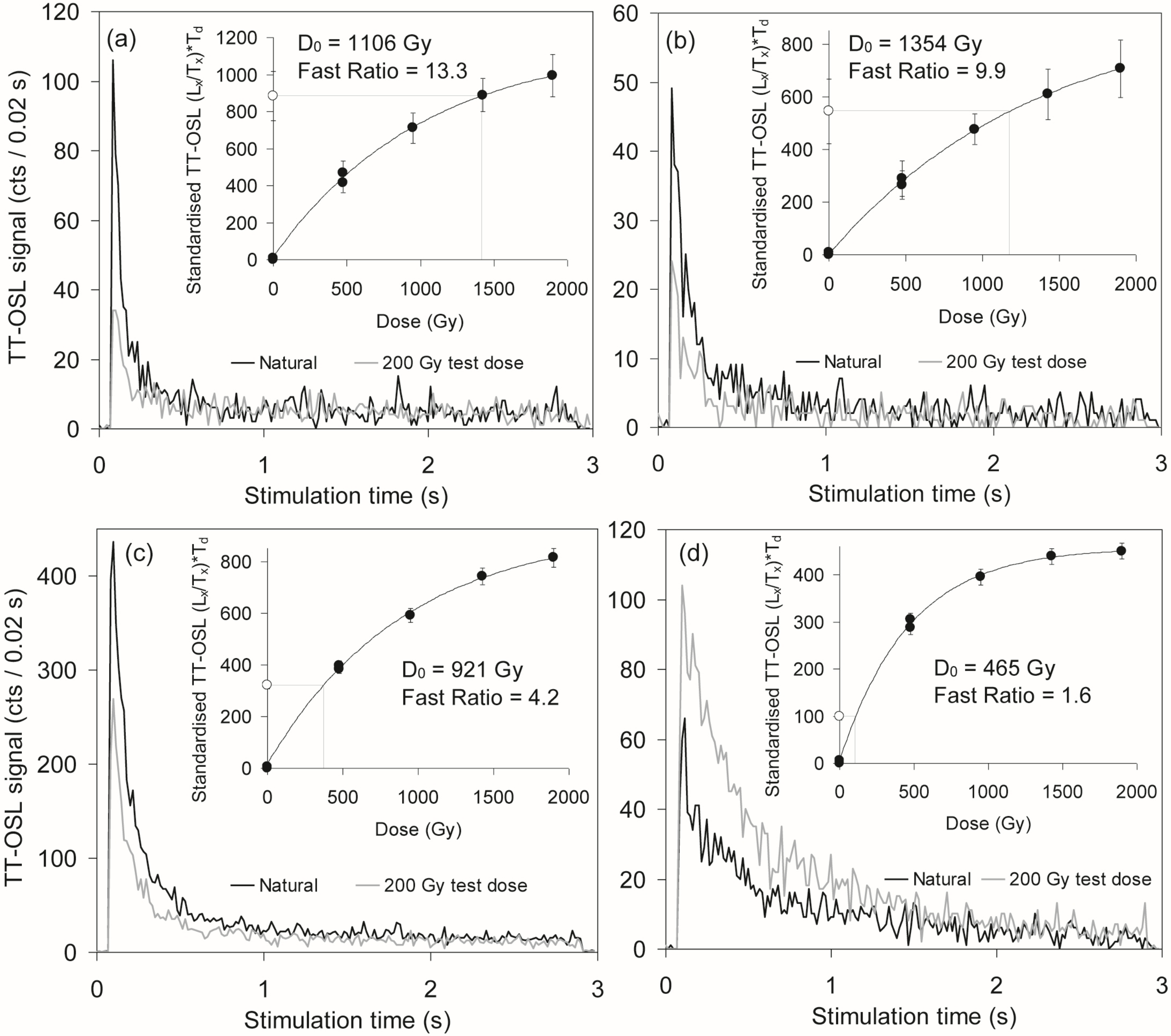

(a)
D0 = 1106 Gy
Fast Ratio = 13.3
Standardised TT-OSL (Lx/Tx)*Td
Dose (Gy)
Natural
200 Gy test dose
TT-OSL signal (cts / 0.02 s)
Stimulation time (s)
(b)
D0 = 1354 Gy
Fast Ratio = 9.9
Standardised TT-OSL (Lx/Tx)*Td
Dose (Gy)
Natural
200 Gy test dose
Stimulation time (s)
(c)
D0 = 921 Gy
Fast Ratio = 4.2
Standardised TT-OSL (Lx/Tx)*Td
Dose (Gy)
Natural
200 Gy test dose
TT-OSL signal (cts / 0.02 s)
Stimulation time (s)
(d)
D0 = 465 Gy
Fast Ratio = 1.6
Standardised TT-OSL (Lx/Tx)*Td
Dose (Gy)
Natural
200 Gy test dose
Stimulation time (s)

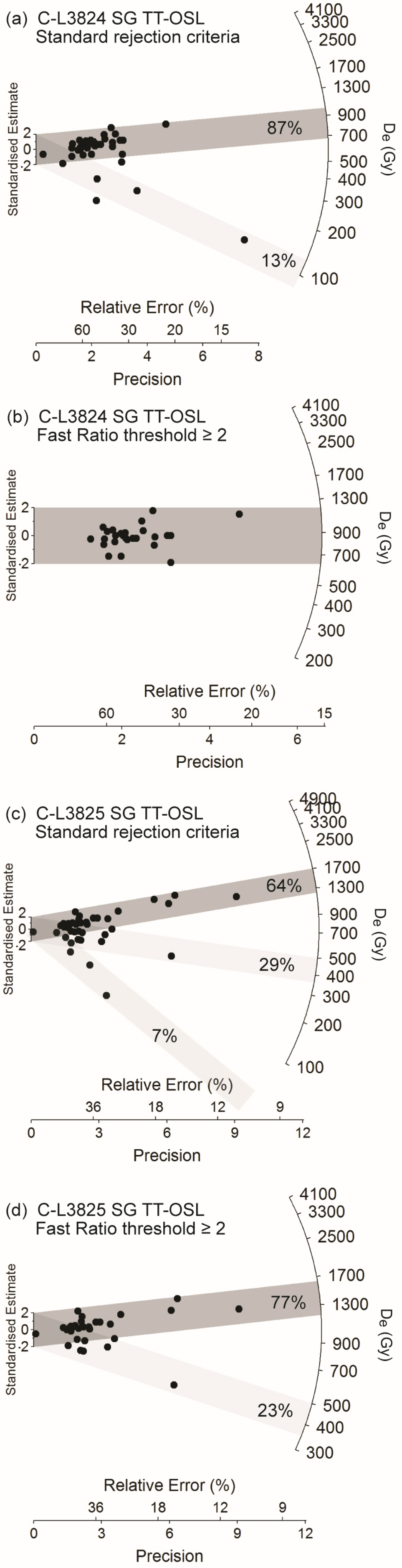
(a) C-L3824 SG TT-OSL
Standard rejection criteria
Standardised Estimate
2
0
-2
87%
13%
4100
3300
2500
1700
1300
900
700
500
400
300
200
100
De (Gy)
Relative Error (%)
60
30
20
15
0
2
4
6
8
Precision
(b) C-L3824 SG TT-OSL
Fast Ratio threshold ≥ 2
Standardised Estimate
2
0
-2
4100
3300
2500
1700
1300
900
700
500
400
300
200
De (Gy)
Relative Error (%)
60
30
20
15
0
2
4
6
Precision
(c) C-L3825 SG TT-OSL
Standard rejection criteria
Standardised Estimate
2
0
-2
64%
29%
7%
4900
4100
3300
2500
1700
1300
900
700
500
400
300
200
100
De (Gy)
Relative Error (%)
36
18
12
9
0
3
6
9
12
Precision
(d) C-L3825 SG TT-OSL
Fast Ratio threshold ≥ 2
Standardised Estimate
2
0
-2
77%
23%
4100
3300
2500
1700
1300
900
700
500
400
300
De (Gy)
Relative Error (%)
36
18
12
9
0
3
6
9
12
Precision

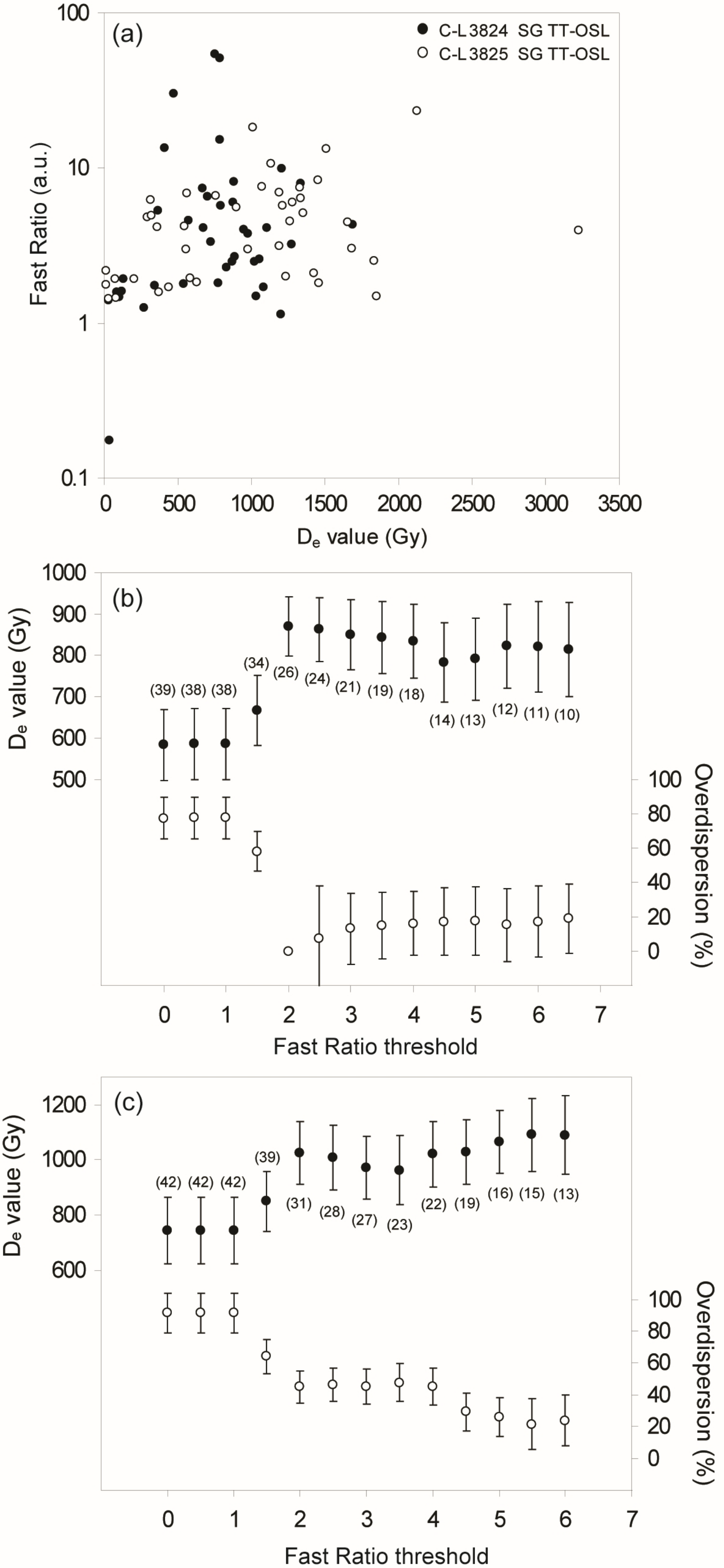

(a)
C-L3824 SG TT-OSL
C-L3825 SG TT-OSL
Fast Ratio (a.u.)
100
10
1
0.1
0
500
1000
1500
2000
2500
3000
3500
D_e value (Gy)
(b)
D_e value (Gy)
1000
900
800
700
600
500
(39) (38) (38)
(34)
(26)
(24)
(21)
(19)
(18)
(14) (13)
(12)
(11) (10)
Overdispersion (%)
100
80
60
40
20
0
0
1
2
3
4
5
6
7
Fast Ratio threshold
(c)
D_e value (Gy)
1200
1000
800
600
(42) (42) (42)
(39)
(31)
(28)
(27)
(23)
(22)
(19)
(16)
(15)
(13)
Overdispersion (%)
100
80
60
40
20
0
0
1
2
3
4
5
6
7
Fast Ratio threshold

	Profile		**BOU**	
	Sample ID	C-L3824	C-L3825	C-L3826[(4)]
Unit	Grain size (µm)	100-150	100-150	100-150
	Depth (m b.s.) [(1)]	5.3	1.5	0.5
Dose rate (Gy/ka)	Total [(2)]	0.80±0.03	1.21±0.05	0.94±0.04
D_e (Gy)	TT-OSL	871±72	1388±109	-
Age (Ma)	TT-OSL	1.09±0.10	1.15±0.10	-
	ESR [(3,4)]	1.26±0.10*	1.10±0.11	1.13±0.09
	pIR_{225} [(4)]	>0.80	-	-
	pIR_{290} [(4)]	-	-	>0.63

[(1)] Actual depth in metres below surface (m b.s.).
[(2)] Values obtained for TT-OSL calculations. Details about the dose rate components can be found in supplementary material (Tab. S2).
[(3)] Based on the Ti centre (asterisk) or the weighted mean D_e values derived from both Al and Ti centres (cf., Bartz et al., 2018).
[(4)] cf. Bartz et al. (2018).

Supplementary material

Single-grain TT-OSL dating results confirm an Early Pleistocene age for the lower Moulouya River deposits (NE Morocco)

M. Bartz[1*], L.J. Arnold[2], M. Demuro[2], M. Duval[3], G.E. King[4], G. Rixhon[5], C. Álvarez Posada[6], J.M. Parés[6] and H. Brückner[1]

Sample preparation

The samples analysed in the present study (C-L3824 and C-L3825) were prepared under subdued red light conditions following the standard luminescence dating procedure at the Cologne Luminescence Laboratory (CLL, University of Cologne), as described in Bartz et al. (2018). After wet sieving, coarse-grained (100-200 µm) sediments were treated with H_2O_2 (10 %), HCl (10 %) and sodium oxalate to remove carbonates, organic material and clay remains. Density separation with sodium polytungstate was used to isolate quartz fractions (ρ_1 = 2.62-2.68 g/cm^3). The resulting quartz minerals were etched with HF (40 %) for 40 min, and subsequently washed with HCl (10 %). Finally, the etched quartz samples were sieved to grain sizes of 100-150 µm.

Measurement equipment and luminescence dating procedure

Single grain TT-OSL signals were optically stimulated using a focussed 10 mW green (532 nm) laser (stimulation power density at sample position ~45 W/cm^2), and detected in the UV-blue spectrum using a 7.5 mm-thick Hoya U 340 glass filter. Single-grain TT-OSL measurements were made by loading 100–150 µm grains into standard single-grain aluminium discs drilled with an array of 300 µm x 300 µm holes. At this resolution, it is estimated that ~12 grains were placed in each grain-hole position (Arnold et al., 2012). However, we are reasonably confident that true single-grain resolution has been maintained in this study because of the particularly low frequency of grain-hole positions that produced

TT-OSL signals when using this configuration (84–86 % of grain-hole positions did not produce any statistically distinguishable TT-OSL T_n signal when measuring ~12 grains per hole).

The single-grain TT-OSL SAR protocol (Tab. S1; Arnold et al., 2014) is based on the multi-grain aliquot approach proposed by Stevens et al. (2009) and makes use of a TT-OSL test dose correction for sensitivity changes, following the same single-grain suitability assessments performed by Arnold et al. (2014, 2015) and Demuro et al. (2014, 2015). Sensitivity-corrected dose-response curves were constructed using the first 0.17 s of each green laser stimulation after subtracting a mean background count obtained from the last 0.25 s of the TT-OSL signal.

Tab. S1: Single-aliquot regenerative (SAR) protocol used for single-grain (SG) TT-OSL D_e determination (Arnold et al., 2014). The SAR measurement cycle was repeated for the natural dose, four different sized regenerative doses, a 0 Gy regenerative dose (to measure OSL signal recuperation) and a replicate of the first regenerative dose cycle (to assess the suitability of the test dose sensitivity correction). The OSL IR depletion ratio of Duller (2003) was measured separately and used to check for the presence of feldspar contaminants.

SG TT-OSL (Arnold et al., 2014)		
Step	Treatment	Signal
1	Dose (natural or laboratory)	
2	Preheat 1 (260 °C for 10 s)	
3	SG OSL stimulation (125 °C for 3 s)	
4	Preheat 2 (260 °C for 10 s)	
5	SG TT-OSL stimulation (125 °C for 3 s)	Ln or Lx
6	OSL stimulation (280 °C for 400 s)	
7	Test dose (200 Gy)	
8	Preheat 3 (260 °C for 10 s)	
9	SG OSL stimulation (125 °C for 3 s)	
10	Preheat 4 (260 °C for 10 s)	
11	SG TT-OSL stimulation (125 °C for 3 s)	Tn or Tx
12	OSL stimulation (290 °C for 400 s)	
13	Repeat measurement cycle for 4 different sized regenerative doses, 0 Gy dose (recuperation ratio), and repeated dose (recycling ratio).	

The Fast Ratio (FR) (Durcan and Duller, 2011; Duller, 2012) has been used to provide a proxy for TT-OSL charge transfer into the fast OSL component trap relative to the medium and slow OSL component traps, as well as for identifying the dominance of potentially interfering (non-transferred) residual slow OSL components in the TT-OSL signals. It is acknowledged that reliable application of the Fast Ratio (FR) to single-grain datasets is potentially complicated by the non-constant optical power densities delivered to different grains during optical stimulation (i.e., dissimilarities in direct and backscattered illumination densities related to variable grain geometries, grain surface properties, grain orientation, positioning and packing within individual grain-hole positions and reproducibility of the single-grain laser system). However, in the present study the FR has primarily been used as a quantitative means of identifying very slowly decaying TT-OSL signals, which are less likely to be explained solely by minor variations in optical stimulation conditions.

Dose rate evaluation and age calculation

Radioelement activities (U, Th and K) were obtained by high-resolution γ-spectrometry (HRGS) analysis and ICP-MS analysis, with the former being used to calculate the final dose rates and ages for the two samples considered in this study (cf., Bartz et al., 2018). The software DRAC v1.2 (Durcan et al., 2015) was used for dose rate and age calculation using the conversion factors of Guérin et al. (2011), and the alpha and beta attenuation factors of Bell (1980) and Guérin et al. (2012), respectively. The thickness of exterior grain surface removed by HF etching was assumed to be 20±10 µm. Water contents of 15±5 % were used in the dose rate calculations (Bartz et al., 2018). The cosmic dose rate contribution was assessed following the approach of Prescott and Hutton (1994), taking into account the altitude, latitude and longitude of the section, as well as the thickness and density of overlying sediments. The latter was assumed to be 1.90±0.05 g cm^{-3}. For a matter of consistency with the previous study by Bartz et al (2018), we used the same values for most of the parameters of dose rate calculations, with two exceptions given the differences between luminescence and ESR signals: an alpha efficiency of 0.04±0.01 was taken from Rees-Jones and Tite (1997), and an internal dose rate of 0.02±0.01 was considered based on Vandenberghe et al. (2008).

Tab. S2: Dose rate and age datasets. Summary of radionuclide activities of uranium (U), thorium (Th) and potassium (K) determined by high-resolution γ-spectrometry (HRGS) (cf., Bartz et al., 2018). DRAC v1.2 (Durcan et al., 2015) was used for dose rate and age calculation, with the conversion factors of Guérin et al. (2011), and alpha and beta attenuation factors of Bell (1980) and Guérin et al. (2012) for quartz. The cosmic dose rate contribution was assessed following the approach of Prescott and Hutton (1994).

	Profile	**BOU**	
	Sample ID	C-L3824	C-L3825
Unit	Grain size (µm)	100-150	100-150
	Depth (m b.s.) (1)	5.3	1.5
	Water content (%) (2)	15±5	15±5
HRGS	^{238}U (Bq/kg)	9.33±0.50	17.16±0.87
	^{232}Th (Bq/kg)	6.21±0.45	11.97±0.77
	^{40}K (%)	0.49±0.01	0.65±0.01
Dose rate	Internal (3)	0.02±0.01	0.02±0.01
	Ext. alpha	0.01±0.01	0.03±0.02
	Ext. beta	0.42±0.02	0.61±0.03
	Ext. gamma	0.24±0.01	0.39±0.02
	Cosmic	0.11±0.01	0.17±0.02
	Total (4)	0.80±0.03	1.21±0.05

(1) Actual depth in metres below surface (m b.s.).
(2) Assumed water content (Bartz et al., 2018).
(3) Assumed internal dose rate following Vandenberghe et al. (2008).
(4) Total dose rate includes an assumed a-value of 0.04±0.01 (Rees-Jones and Tite, 1997).

Single-grain TT-OSL results

Tab. S3: Single-grain OSL classification statistics. The proportion of grains that were rejected from the final D_e estimation after applying the various SAR quality assurance criteria of Arnold et al. (2014) are shown in rows 6-13.

Sample name	**C-L3824**	**C-L3825**	**C-L3824**
SAR measurement type	D_e	D_e	Dose-recovery
Total measured grains	1600	1000	900
Reason for rejecting grains from D_e analysis			
Standard SAR rejection criteria:	%	%	%
T_n <3σ background	88	86	84
Recycling ratio ≠ 1 at ±2σ	3	3	3
OSL-IR depletion ratios <1 at ±2σ	0	0	0
0 Gy L_x/T_x >5% L_n/T_n	0	0	0
Non-intersecting grains (L_n/T_n > dose response curve saturation)	0	0	0
Saturated grains (L_n/T_n ≥ dose response curve I_{max} at ±2σ)	0	0	0
Extrapolated grains (L_n/T_n > highest L_x/T_x at ±2σ)	0	0	0
Anomalous dose response / unable to perform Monte Carlo fit	7	7	9
Sum of rejected grains (%)	98	96	96
Sum of accepted grains (%)	2	4	4

Tab. S4: Single-grain TT-OSL D_e summary statistics and final ages for samples C-L3824 and C-L3825.

Sample	Grain size (µm)	Total dose rate (Gy/ka) [1]	Equivalent dose (D_e) data								TT-OSL age (ka) [8] [9]
			SAR rejection criteria [2]	***n* / *N*** [3]	**Weighted skewness** [4]	**Critical skewness (95 % C.I.)** [5]	**Overdis-persion (%)**	**Age Model** [6] [7]	**Proportion of grains (%)**	**D_e (Gy)** [1]	
C-L3824	100-150	0.80 ± 0.03	Standard	39 / 1600	-1.71	± 0.78	77 ± 12	FMM comp. 1 (K_1)	13 ± 6	103 ± 16	128.6 ± 20.5
								FMM comp. 2 (K_2)	87 ± 6	818 ± 67	1022.2 ± 94.4
			Standard + FR threshold = 2	26 / 1600	-0.39	± 0.96	0 ± 0	CAM	100	871 ± 72	**1088.3 ± 101.1**
C-L3825	100-150	1.21 ± 0.05	Standard	42 / 1000	-1.77	± 0.76	91 ± 13	FMM comp. 1 (K_1)	7 ± 4	43 ± 10	35.7 ± 8.5
								FMM comp. 2 (K_2)	29 ± 10	424 ± 63	350.3 ± 54.2
								FMM comp. 3 (K_3)	64 ± 10	1426 ± 108	1178.2 ± 104.1
			Standard + FR threshold = 2	31 / 1000	-1.02	± 0.88	45 ± 10	FMM comp. 1 (K_1)	23 ± 10	422 ± 71	348.8 ± 60.5
								FMM comp. 2 (K_2)	77 ± 10	1388 ± 109	**1146.8 ± 104.2**

(1) Mean ± total uncertainty (68 % confidence interval), calculated as the quadratic sum of the random and systematic uncertainties.
(2) Standard = routine quality assurance criteria used by Arnold et al. (2014); Standard + FR threshold = An additional Fast Ratio threshold criterion has been added to the routine quality assurance criteria to ensure that the accepted grain populations exhibit rapidly decaying TT-OSL signals. Suitable Fast Ratio threshold values have been determined for each sample using the data shown in fig. 3**.**
(3) Number of D_e measurements that passed the SAR rejection criteria (*n*) / total number of D_e values measured (*N*).
(4) Weighted skewness scores have been calculated on log-transformed D_e values (using Eq. 7-8 of Arnold and Roberts, 2009) in accordance with the multiplicative error properties of these datasets.
(5) Critical skewness scores have been calculated using Eq. 16 of Bailey and Arnold (2006). D_e distributions are considered to be significantly skewed if the weighted skewness value is greater than the corresponding critical skewness value. Critical skewness values are taken to be equivalent to twice the standard error of skewness score for these single-grain D_e datasets, following the results of sensitivity analyses performed by Bailey and Arnold (2006) and Arnold et al. (2007).
(6) CAM = central age model (Galbraith et al., 1999), FMM = finite mixture model (Galbraith and Green, 1990).
(7) The FMM was fitted by varying the common overdispersion parameter (σ_k) between 5 and 25 % and incrementally increasing the specified number of k_n components. The FMM parameter values shown here were obtained from the optimum FMM fit (i.e., the fit with the lowest BIC score; Arnold and Roberts, 2009), which corresponded to a σ_k value of 15 % for sample C-L3824 and 10 % for sample C-L3825 (consistent with the empirical overdispersion values obtained for well-bleached, unmixed TT-OSL D_e datasets; Arnold et al., this volume). Using this approach, the D_e distributions of sample C-L3824 and C-L3825 are shown to contain two and three discrete dose populations, respectively, when applying the standard SAR rejection criteria. Application of an additional Fast Ratio threshold eliminates the lowest dose populations of both samples.
(8) Total uncertainty includes a systematic component of ±2 % associated with laboratory beta-source calibration.
(9) The preferred ages are shown in bold for each sample (see text for further details).

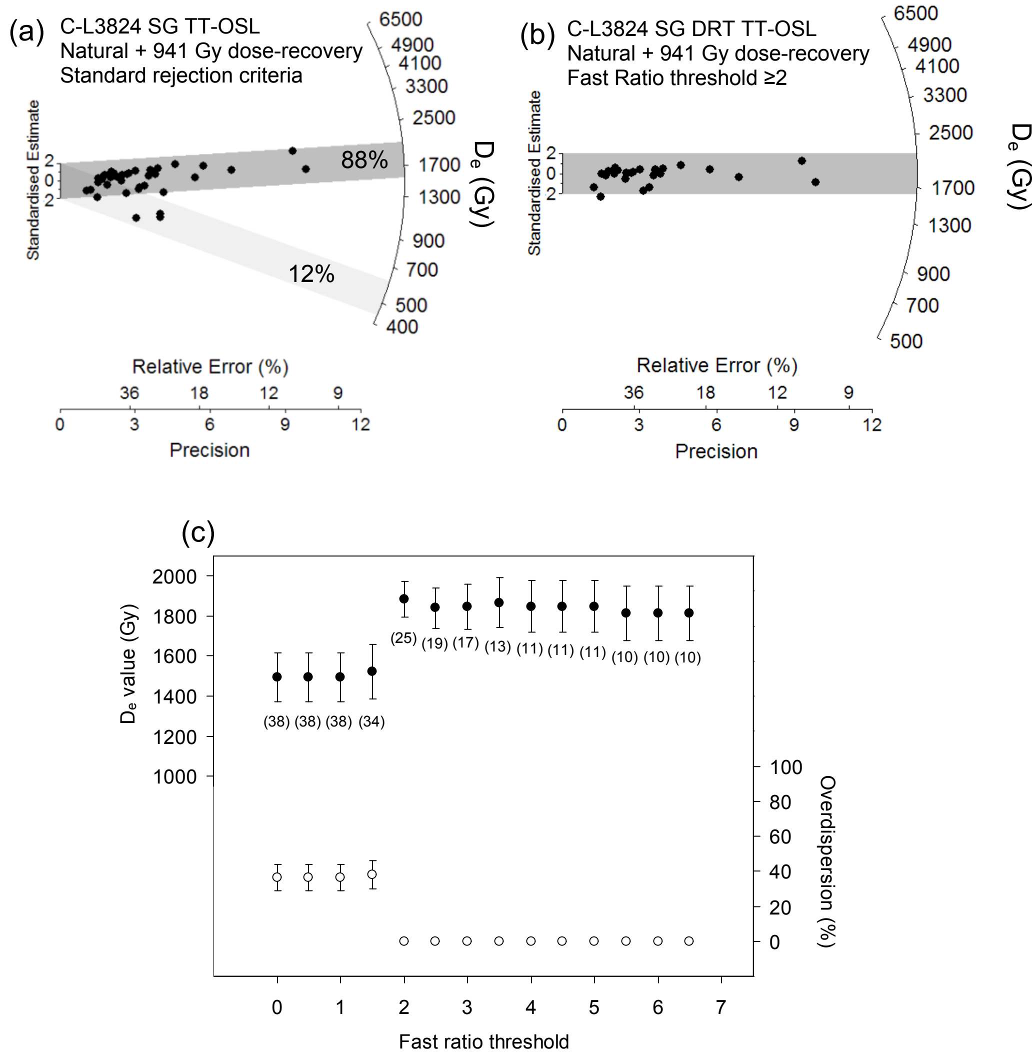

Fig. S1: Single-grain TT-OSL dose-recovery test results for samples C-L3824. (a) Radial plot showing the dose-recovery test (natural + dosed) D_e values obtained for sample C-L3824 after applying the routine SAR quality assurance criteria of Arnold et al. (2014). (b) Radial plot showing the dose-recovery test (natural + dosed) D_e values obtained for sample C-L3824 after applying an additional Fast Ratio threshold criterion (determined specifically for this D_e dataset using the results shown in fig 4. (c) Plot showing the weighted mean (CAM) D_e and overdispersion values obtained for the C-L3824 dose-recovery dataset when applying different Fast Ratio thresholds. In plot (a), the weighted mean burial dose estimate of the dominant FMM component (i.e., that containing the highest proportion of individual D_e values) is shown as a dark grey shaded band on the radial plot. The additional dose component identified by the optimum FMM fit is shown as a light grey shaded band. The percentage of grains associated with each fitted FMM component is also shown on the radial plot. In plot (b), the grey band is centred on the weighted mean D_e value, determined using the central age model of Galbraith et al. (1999). In plot (c), progressively higher Fast Ratio thresholds have been applied to the dose-recovery D_e dataset, starting at a Fast ratio of 0 and increasing in Fast Ratio increments of 0.5 until the culled dataset contained fewer than 10 individual D_e values (i.e., the sample size became too limited to ensure precise single-grain D_e determination). In each instance, grains were only accepted for further D_e analysis if their individual Fast Ratio value equalled or exceeded the corresponding threshold shown on the x-axis. The values shown in brackets represent the number of grains remaining in the D_e dataset after applying each Fast Ratio threshold criterion.

References

Arnold, L.J., Demuro, M., Navazo Ruiz, M., 2012. Empirical insights into multi-grain averaging effects from ‘pseudo’ single-grain OSL measurements. Radiation Measurements 47, 652–658.

Arnold, L.J., Demuro, M., Parés, J.M., Arsuaga, J.L., Aranburu, A., Bermudéz de Castro, J.M., Carbonell, E., 2014. Luminescence dating and palaeomagnetic age constraint on hominins from Sima de los Huesos, Atapuerca, Spain. Journal of Human Evolution 67, 85-107.

Arnold, L.J., Demuro, M., Parés, J.M., Pérez-González, A., Arsuaga, J.L., Bermúdez de Castro, J.M., Carbonell, E., 2015. Evaluating the suitability of extended-range luminescence dating techniques over early and Middle Pleistocene timescales: Published datasets and case studies from Atapuerca, Spain. Quaternary Geochronology 389, 167-190.

Bailey, R.M., Arnold, L.J., 2006. Statistical modelling of single grain quartz D_e distributions and an assessment of procedures for estimating burial dose. Quaternary Science Reviews 25, 2475-2502.

Bartz, M., Rixhon, G., Duval, M., King, G.E., Álvarez Posada, C., Parés, J.M., Brückner, H., 2018. Successful combination of electron spin resonance, luminescence and palaeomagnetic dating methods allows reconstruction of the Pleistocene evolution of the lower Moulouya river (NE Morocco). Quaternary Science Reviews 185, 153-171.

Bell, W.T., 1980. Alpha dose attenuation in quartz grains for thermoluminescence dating. Ancient TL 12, 4-8.

Demuro, M., Arnold, L.J., Parés, J.M., Pérez-González, A., Ortega, A.I., Arsuaga, J.L., Bermúdez de Castro, J.M., Carbonell, E., 2014. New luminescence ages for the Galería Complex Archaeological Site: Resolving chronological uncertainties on the Acheulean record of the Sierra de Atapuerca, Northern Spain. PLoS ONE 9 (10), 110-169.

Demuro, M., Arnold, L.J., Parés, J.M., Sala, R., 2015. Extended-range luminescence chronologies suggest potentially complex bone accumulation histories at the Early-to-Middle Pleistocene palaeontological site of Huéscar-1 (Guadix-Baza basin, Spain). Quaternary International 389, 191-212.

Duller, G.A.T., 2003. Distinguishing quartz and feldspar in single grain luminescence measurements. Radiation Measurements 37, 161-165.

Duller, G.A.T., 2012. Improving the accuracy and incision of equivalent doses determined using the optically stimulated luminescence signal from single grains of quartz. Radiation Measurements 47, 770-777.

Durcan, J.A., Duller, G.A.T., 2011. The fast ratio: A rapid measure for testing the dominance of the fast component in the initial OSL signal from quartz. Radiation Measurements 46, 1065-1072.

Durcan, J.A., King, G.E., Duller, G.A.T., 2015. DRAC: Dose rate and age calculator for trapped charge dating. Quaternary Geochronology 28, 54-61.

Galbraith, R.F., Green, P.F., 1990. Estimating the component ages in a finite mixture. Nuclear Tracks and Radiation Measurements 17 (3), 197-206.

Galbraith, R.F., Roberts, R.G., Laslett, G.M., Yoshida, H., Olley, J.M., 1999. Optical dating of single and multiple grains of quartz from Jinmium rock shelter, northern Australia: Part I, experimental design and statistical models. Archaeometry 41 (2), 339-364.

Guérin, G., Mercier, N., Adamiec, G., 2011. Dose-rate conversion factors: update. Ancient TL, 29, 5-8.

Guérin, G., Mercier, N., Nathan, R., Adamiec, G., Lefrais, Y., 2012. On the use of the infinite matrix assumption and associated concepts: A critical review. Radiation Measurements, 47, 778-785.

Prescott, J.R., Hutton, J.T., 1994. Cosmic ray contributions to dose rates for luminescence and ESR dating: Large depths and long-term time variations. Radiation Measurements 23, 497-500.

Rees-Jones, J., Tite, M.S., 1997. Optical dating results for British archaeological sediments. Archaeometry 39 (1), 177-187.

Stevens, T., Buylaert, J.-P., Murray, A.S., 2009. Towards development of a broadly-applicable SAR TT-OSL dating protocol for quartz. Radiation Measurements 44, 639-645.

Vandenberghe, D., De Corte, F., Buylaert, J.-P., Kučera, J., Van den Haute, P., 2008. On the internal radioactivity in quartz. Radiation Measurements 43, 771-775.